When Shil'nikov meets Hopf in excitable systems

Alan R. Champneys, Vivien Kirk, Edgar Knobloch,
Bart E. Oldeman, James Sneyd

February 8, 2007

Abstract

This paper considers a hierarchy of mathematical models of excitable media in one spatial dimension, specifically the FitzHugh-Nagumo equation and several models of the dynamics of intracellular calcium that have arisen in the work of Sneyd and collaborators. A common feature of the models is that they support solitary travelling pulse solutions which lie on a characteristic C-shaped curve of wave speed versus parameter. This C lies to the left of a U-shaped locus of Hopf bifurcations that corresponds to the onset of small-amplitude linear waves. The central question addressed is how the Hopf and solitary wave (homoclinic orbit in a moving frame) bifurcation curves interact in these 'CU systems.'

A variety of possible codimension-two mechanisms is reviewed through which such Hopf and homoclinic bifurcation curves can interact. These include Shil'nikov-Hopf bifurcations and the local birth of homoclinic chaos from a saddle-node/Hopf (Gavrilov-Guckenheimer) point. Alternatively, there may be barriers in phase space that prevent the homoclinic curve from reaching the Hopf bifurcation. For example, the homoclinic orbit may bump into another equilibrium at a so-called T-point, or it may terminate by forming a heteroclinic cycle with a periodic orbit.

This paper presents the results of detailed numerical continuation results on different CU-systems, thereby illustrating various of the mechanisms by which Hopf and homoclinic curves interact in CU systems. Owing to a separation of time scales in these systems, considerable care has to be taken with the numerics in order to reveal the true nature of the bifurcation curves observed.

1 Introduction

So-called *excitable* systems of reaction-diffusion equations are used to model a variety of biophysical processes, including neuronal information processing, heart electro-physiology and the processes by which cells signal to one another, see e.g. [17, 28]. One of the early successes in mathematical biology was Hodgkin and Huxley's work on modelling a squid giant nerve axon [27], leading to the equations that bear their name. Later in the 1960s FitzHugh [18] and Nagumo [32] came up with a simplified version, which has since come to be considered the canonical excitable system.

The FitzHugh-Nagumo model is called excitable because, in the absence of diffusion a small perturbation from the stable equilibrium causes straightforward relaxation back to the equilibrium, whereas a large enough perturbation causes a sudden, large-amplitude burst followed by slow relaxation. The power of the FitzHugh-Nagumo model arises from the fact that a vast array of physical

and biological systems display phenomenologically similar behaviour. On the face of it, the propagation of a wave of electric potential down a nerve axon, and the spread of a forest fire, share little in common. Mathematical models are powerful because they can abstract the essential behaviours from each of these situations and show how similar they really are.

One recent application of excitable system theory has been to the study of the propagation of waves of increased calcium concentration both within and between cells. In the last 20 years it has become clear that the dynamics of calcium inside cells is responsible for the control of a wide array of cellular processes, and thus calcium waves and oscillations have been studied intensively by both experimentalists and theoreticians. Right from the earliest models it has been recognized that calcium waves propagate by an excitable mechanism essentially the same as that in the FitzHugh-Nagumo model, and thus can be partially understood by the analysis of such simpler excitable systems.

Here, we write the FitzHugh-Nagumo equations in the form

$$
\begin{aligned}
v_t &= \Delta v_{xx} + f_\alpha(v) - w + p \\
w_t &= \varepsilon(v - \gamma w),
\end{aligned}
\tag{1}
$$

where x is a real spatial variable, t represents time and $f_\alpha \equiv v(v-1)(\alpha-v)$. In the original FitzHugh-Nagumo model the variable v represents the plasma membrane electric potential, with diffusion constant Δ, and w is a phenomenological variable representing the combined inactivation effects of potassium and sodium ion channels. The small parameter ε represents the ratio of the time constant of the channels (the channels here act on a slow time scale) to that of the membrane potential (which is a much faster process). The form of f_α is chosen so that, depending on the values of the threshold, α, or applied current, p, there is the possibility of either bi-stability between different spatially homogeneous states or excitability of the background state. (We use p to denote the applied current, rather than the more usual I, so as to maintain consistency with the later models discussed here).

For Δ sufficiently large the background equilibrium state becomes destabilized and the dynamics supports pulse-type travelling waves which are solitary structures that move with a constant wave speed s. Equations (1) in the moving frame take the form

$$
\begin{aligned}
\dot{v} &= d \\
\dot{d} &= \frac{1}{\Delta}(sd - v(v-1)(\alpha-v) + w - p) \\
\dot{w} &= \frac{\varepsilon}{s}(v - \gamma w),
\end{aligned}
\tag{2}
$$

where the dot denotes differentiation with respect to the new variable $z \equiv x + st$. In these equations the background equilibrium is of saddle type, and the travelling pulse in the system (1) corresponds to a homoclinic orbit of this saddle in the moving frame.

In what follows we consider equations (2) for the parameter values

$$
\Delta = 5.0, \quad \alpha = 0.1, \quad \gamma = 1.0, \quad \varepsilon = 0.01,
\tag{3}
$$

with the wave speed, s, and applied current, p, allowed to vary. For these fixed values there is a unique equilibrium point, which is of saddle type with a one-dimensional unstable manifold and a two-dimensional stable manifold provided that s is outside the red curve, $s = s_H(p)$, labelled Hopf in Fig. 1. On the red curve, a Hopf bifurcation occurs and for $s > s_H(p)$ the equilibrium is completely unstable. Since the equilibrium no longer has a stable manifold, it is impossible for a homoclinic
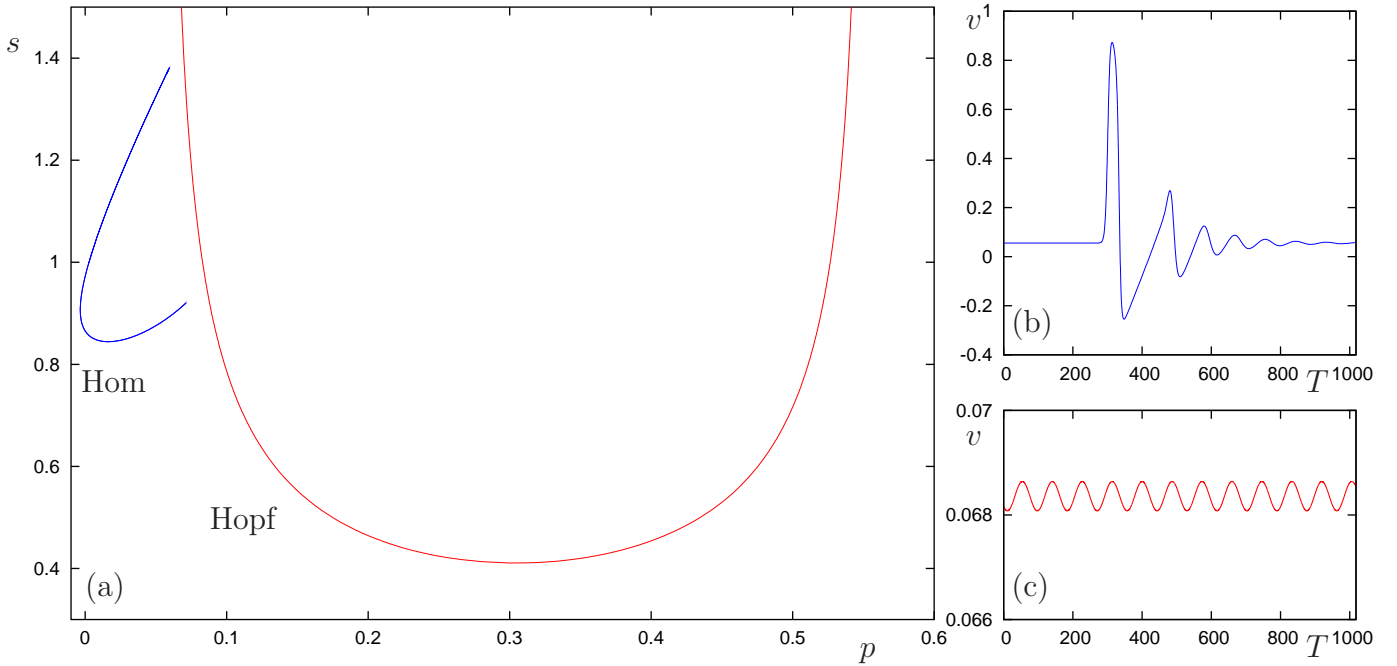
2

Figure 1: (a) Partial bifurcation set for the travelling wave FitzHugh-Nagumo equations (2) for the parameter values given in (3), illustrating the U-shaped curve of Hopf bifurcations and C-shaped curve on which homoclinic orbits occur. Panel (b) shows a time series for a homoclinic orbit near the top of the C branch, at $(p, s) = (0.0575862, 1.37)$. Panel (c) shows a time series for a nearby periodic orbit, at $(p, s) = (0.0703753, 1.37)$; this periodic orbit is created in a Hopf bifurcation on the U branch.

orbit to occur inside the red curve; hence the corresponding solitary pulses in the PDE cannot exist for parameter values inside the U-shaped curve. In fact, careful path-following techniques for homoclinic orbits [12] reveal that solitary pulse solutions lie on a C-shaped curve to the left of the U in the (p, s) parameter plane, which is also depicted in Fig. 1. For more on computations of such travelling wave solutions in various different forms of FitzHugh-Nagumo model, see [11, 36] and references therein. The C-shape of the pulse curve implies that more than one solitary pulse exists for a range of values of p, for two different wave speeds. In general though, it is known that only pulses on the upper, faster branch of the C can be stable.

Although it might seem that this structure, of a C-shaped curve of homoclinic orbits and a U-shaped curve of Hopf bifurcations, would be peculiar to the FitzHugh-Nagumo model, it turns out that a much wider array of excitable models share this same basic feature. Indeed, in every excitable model we have examined so far, including the FitzHugh-Nagumo model, all excitable models of calcium waves, and the Hodgkin-Huxley equations, this same fundamental structure appears. It seems, therefore, that this CU structure is a common feature of excitable systems, reflecting some fundamental underlying property of excitability. In the following we refer to such systems as *CU-systems*.

In addition to the FitzHugh-Nagumo model, we also study here a hierarchy of models of intracellular calcium waves. Although these models were originally developed as a description of calcium waves in pancreatic acinar cells, the underlying CU structure is common to every calcium wave model we have yet studied.

A typical model for intracellular calcium dynamics in one spatial dimension has the form

$$
\begin{aligned}
\frac{\partial c}{\partial t} &= D\frac{\partial^2 c}{\partial x^2} + J_{\text{IPR}}(G, c, p)(c - c_e) - J_{\text{serca}} + \delta(J_{\text{in}} - J_{\text{pm}}) \\
\frac{dc_e}{dt} &= -J_{\text{IPR}}(G, c, p)(c - c_e) + J_{\text{serca}} \\
\frac{dG}{dt} &= k_3(p, c)G,
\end{aligned}
$$

where c denotes the concentration of free calcium in the cell cytoplasm, c_e denotes the concentration of free calcium in the endoplasmic reticulum (ER), and G denotes a set of gating variables that describe the time-dependent behaviour of the calcium release channel, the so-called inositol trisphosphate receptor, or IPR. The variables G are exactly analogous to the variables m, n and h in the Hodgkin-Huxley model, or to the variable w in the FitzHugh-Nagumo model. The parameter p denotes the concentration of the second messenger inositol trisphosphate (IP$_3$). IP$_3$ is produced as a result of stimulation by hormones or neurotransmitters, and is the second messenger that controls the release of calcium from the ER, via the IPR. In all the calcium wave models we study here, p will be treated as a bifurcation parameter. In general, it can be manipulated experimentally, by changing the level of stimulation applied to the cell. In some cell types p is also a dynamic variable, with its rates of production and degradation controlled by calcium. Although we do not consider any such models here, preliminary computations show them to have the same CU structure, and thus our results should be applicable to that class of models also.

The Js denote various calcium fluxes into and out of the cytoplasm and ER. For instance, J_{serca} denotes the flux of calcium through ATPase calcium pumps on the membrane of the ER. These pumps move calcium up its concentration gradient from the cytoplasm to the ER, consuming ATP in the process. J_{in} is a leak of calcium from the outside of the cell into the cytoplasm, J_{pm} is the flux of calcium through plasma membrane ATPase calcium pumps, while J_{IPR} is the flux of calcium through the IPR. Note that J_{IPR} depends on G, c and p, as these are the three major controllers of the IPR.

Within this overall class of calcium wave models there is huge variety. For a start, there are many different expressions for each of the various flux terms; the particular one chosen depends on many factors, but is most strongly influenced by the available experimental data and by the goal of the model. In addition, there may be many gating variables, G, or only a few. Although complicated Markov models of the IPR, with many different states, are sometimes used to derive the differential equations for G, these complex models can often be simplified by assuming fast transitions between various states, leading to simpler models with fewer gating variables. Here, we study a variety of models, ranging from a model with a single gating variable to a model with seven gating variables.

Readers interested in the process of model construction and simplification are referred to the original papers. Here we shall merely state the model equations and their parameters.

An aim of this paper is to identify the ways in which the C-shaped curve of homoclinic orbits can terminate, either at or before it reaches the U-shaped curve of Hopf bifurcations. For example, in Fig. 1, it may seem that the computation of the curve of homoclinic bifurcations shown in the figure has been abnormally terminated, since topological considerations demand that a bifurcation curve cannot end 'in mid air' unless it is at a codimension-two point. In fact, as we shall see in Sec. 3.1 below there is a rational explanation of this apparent termination, which to our knowledge has not been reported in the literature. More generally, a detailed understanding of how the C and U curves interact is crucial for an understanding of wave structure in these excitable models. For lower values of p in Fig. 1 the model supports a stable traveling pulse solution, but as p increases, these

pulse solutions become unstable and, inside the U curve, turn into periodic plane waves. Thus, in order to understand how pulse waves turn into periodic waves, we must first understand the ways in which the C curve can terminate, either at or before the U curve. Since, in all the models we consider here, the parameter p is one that can be controlled experimentally, it is plausible that theoretical predictions about the transition from pulse to periodic waves will be able to be tested experimentally. However, such considerations are left for future work, as a proper mathematical understanding is a prerequisite for the development of testable predictions.

For each model, we shall carry out a detailed numerical bifurcation analysis in order to elucidate the way in which the homoclinic curve terminates. We will show that homoclinic branches can terminate in quite different ways in different systems. First of all, the mechanism involved depends on whether the Hopf bifurcation is subcritical or supercritical at the point where the homoclinic bifurcation curve approaches, but even with this knowledge there are several possibilities, and the only way to determine what is going on is using numerical techniques. These investigations have helped us identify five different codimension-two mechanisms by which a branch of homoclinic bifurcations of an equilibrium may be terminated in a CU system: a Shil'nikov-Hopf bifurcation; an equilibrium-to-equilibrium heteroclinic cycle (the so-called T-point); a local saddle-node/Hopf bifurcation; a codimension-two heteroclinic cycle between an equilibrium and a periodic orbit; and a tangency in a codimension-one equilibrium-to-periodic heteroclinic cycle. Termination via a heteroclinic cycle between an equilibrium and a fold of limit cycles is also possible, but this mechanism has not yet been seen in a CU system.

The rest of the paper is organized as follows. Section 2 gives a brief overview of homoclinic bifurcation theory, and in particular of some codimension-two mechanisms which can terminate a branch of homoclinic orbits as it approaches a Hopf bifurcation. Relevant references to the literature are given to where full unfoldings may be found, or, in the case of at least two of the mechanisms, to forthcoming analysis by some of the present authors that will provide just such detail. Section 3 contains the main contribution of this paper, that is the presentation of careful numerical continuation results that reveal the specifics of the bifurcation diagrams for each of the six example systems. Finally, Section 4 attempts to draw general lessons from these numerical results. Tentative explanations are also offered for previously-reported 'anomalous' Shil'nikov-Hopf bifurcations, where a homoclinic curve appears to pass straight through the Hopf curve, in defiance of theory, a 'ghost' phenomenon that appears to be due to the slow-fast nature of excitable systems.

2   Homoclinic bifurcations

This section introduces notation and reviews results about homoclinic bifurcations from the existing literature. See, for instance, [29, 39] and references therein for full details.

2.1   Codimension-one Shil'nikov homoclinic bifurcation

Consider a continuous-time dynamical system

$$\dot{u} = f(u, p), \quad u \in \mathbb{R}^n, \quad p \in \mathbb{R}^m,$$

and assume there is a hyperbolic equilibrium point $u_0(p)$ which for a codimension-one set of parameter values has an isolated homoclinic orbit H_1 that connects its stable and unstable manifolds. The dynamical behaviour of orbits near the homoclinic orbit depends, among other things, on the
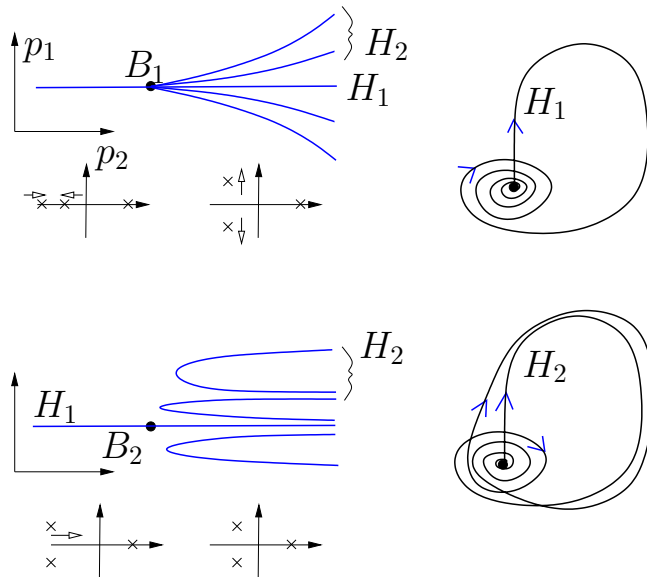
Figure 2: Partial unfoldings of two Belyakov transitions in the (p_1, p_2) parameter plane. Here p_1 unfolds the existence of a primary homoclinic orbit H_1 whereas variation of p_2 causes the homoclinic bifurcation to change from the tame case to the Shil'nikov case. In the upper panel, the Belyakov point B_1 is caused by a pair of non-semisimple eigenvalues coalescing on the real axis and becoming complex. In the lower panel the saddle quantity σ changes sign. In both cases, infinitely many N-pulse homoclinic orbits are created in the neighbourhood of the B-points, represented here by a few curves of double-pulses H_2. There are also infinitely many curves of period-doublings and folds of periodic orbits that are not depicted.

eigenvalues of the flow linearized about the equilibrium. The *leading* eigenvalues of the equilibrium are defined as the eigenvalues of $f_u(u_0(p), p)$ that have positive and negative real part closest to zero. From now on, we assume that the leading eigenvalues of the equilibrium involved in the homoclinic bifurcation consist of a real, positive eigenvalue $\lambda > 0$ and a pair of complex conjugate eigenvalues $-\mu \pm i\omega$, $\mu > 0$. This is precisely the eigenvalue structure characteristic of the equilibrium to the left (of the left arm) of the U-shaped Hopf curve in all of the examples that follow.

The saddle quantity $\sigma = \lambda - \mu$ is defined as the sum of the real parts of the leading stable and the leading unstable eigenvalues. If $\sigma < 0$ then the homoclinic bifurcation upon varying a parameter is tame and involves finitely many periodic orbits in a neighbourhood of the homoclinic orbit in both phase and parameter space. The case of prime interest here is the so-called Shil'nikov behaviour that occurs when $\sigma > 0$. This case involves shift dynamics on infinitely many symbols which implies in particular the existence of infinitely many periodic orbits that have arbitrarily long periods of spiralling behaviour close to u_0. Moreover, there are sequences of nearby parameter values at which there exist double pulse homoclinic orbits H_2 that make two large excursions in a neighbourhood of the primary homoclinic orbit. In addition there are infinitely many N-pulse homoclinic orbits for all positive integers N.

A number of codimension-two mechanisms have been observed in which the dynamics in a neighbourhood of H_1 changes qualitatively; see [11] for a partial review. For example, the saddle quantity can change sign as we vary parameters along a homoclinic bifurcation curve in the parameter plane. Such a transition is called a Belyakov bifurcation, after the Russian mathematician who first described this situation [1]. A schematic representation of what occurs in such a codimension-two bifurcation is depicted in the lower portion of Fig. 2. Another kind of Belyakov bifurcation [2]

occurs when the complex pair of leading eigenvalues associated with the equilibrium undergoing a homoclinic bifurcation becomes real, so that a saddle-focus becomes a saddle. This latter transition, which is depicted in the upper part of Fig. 2 is the one that we encounter in this paper. Associated with this type of Belyakov transition is the birth of multi-pulse homoclinic orbits; these orbits enter and then leave a neighbourhood of the equilibrium one or more times before converging back to the equilibrium. Codimension-one curves of multi-pulse homoclinic orbits emanate from the codimension-two Belyakov point.

Neither of these codimension-two bifurcations produces an end-point on the C-shaped homoclinic branch. The question we wish to address is just how this termination happens as the C approaches the U in the systems we investigate. Naively, one might expect that this would occur via the so-called Shil'nikov-Hopf bifurcation (see Fig. 3) that occurs as the complex eigenvalues of the Shil'nikov equilibrium cross the imaginary axis. However, as summarized in the next section, there are other possibilities as well.

2.2   Possible codimension-two termination mechanisms

Figure 3 depicts partial unfoldings of six different codimension-two mechanisms by which a branch of homoclinic orbits to an equilibrium may terminate as it approaches a Hopf bifurcation curve in a parameter plane. We describe below the dynamics corresponding to each of the panels in the figure. Note that this list is not exhaustive, but is specific to the case found in the CU systems considered here where there is an equilibrium that has a one-dimensional unstable manifold to the left of the U-shaped Hopf curve. In particular, in Section 3 below we shall find examples of at least four of these mechanisms in the CU systems we consider.

The six cases are:

(a) A Shil'nikov-Hopf bifurcation. This codimension-two point occurs when the equilibrium to which the homoclinic orbit is connected undergoes a supercritical Hopf bifurcation. On the far side of the Hopf bifurcation, the parameter curve of homoclinic orbits transforms into a heteroclinic cycle that connects the equilibrium to the small amplitude limit cycle born at the Hopf bifurcation. There is also a parabolic curve on which homoclinic tangencies to the periodic orbit exist. Inside the parabola there are shift dynamics on infinitely many symbols. This situation was also first analysed by Belyakov [3], with more complete treatments appearing in the work of Hirschberg & Knobloch [26] and Deng & Sakamoto [13].

(b) A fold-Hopf (or saddle-node Hopf) bifurcation occurs when a pure imaginary pair and a zero eigenvalue occur in the linearisation about the equilibrium. See [29] and references therein for details of the unfolding of this codimension-two local bifurcation. There are several cases, depending on the signs of certain nonlinear terms in the two-dimensional normal form. In the so-called $(+, -)$ case, it is inevitable that two small-amplitude homoclinic orbits originate from this codimension-two bifurcation [5, 19], doing so with a characteristic entwined wiggling in the parameter space, see [8].

(c) A T-point [25] (or Bykov point [6, 7]). This is an equilibrium-to-equilibrium codimension-two heteroclinic cycle, and two branches of primary homoclinic orbits bifurcate from it. If one equilibrium is a saddle-focus with a negative saddle index and the other has real eigenvalues, then one curve of homoclinic orbits spirals in parameter space, while the other approaches the T-point monotonically. Such a T-point may or may not appear close to a Hopf bifurcation in parameter space.
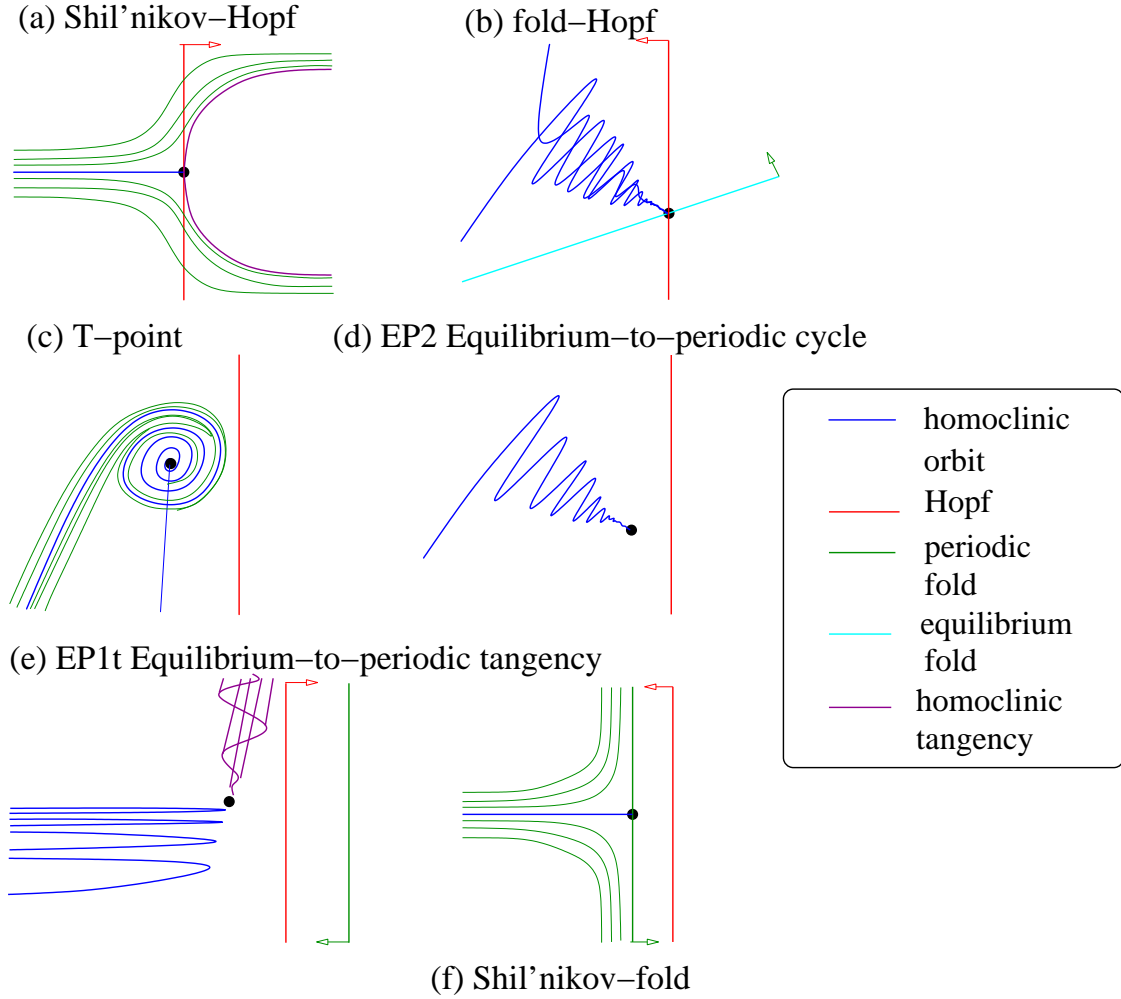
7

Figure 3: Qualitative unfolding diagrams of six different codimension-two mechanisms that could cause the termination of the homoclinic branch (blue curve) in a CU-system, as it approaches the (red) Hopf curve. The arrows in the figure denote the direction in which the periodic orbit bifurcates from the Hopf bifurcation or from other key bifurcation curves. Note that in full unfoldings of each case there are many more bifurcation curves than those depicted. See text for more details.

(d) Equilibrium-to-periodic heteroclinic cycle (EP2 point). At such a point there exists a heteroclinic cycle consisting of a connection from an equilibrium to a periodic orbit and a connection from the periodic orbit back to the equilibrium. In the case that the unstable manifold of the equilibrium is one-dimensional, we require that the periodic orbit has a three-dimensional unstable manifold and an $(n-2)$-dimensional stable manifold. Then the heteroclinic connection *from* the equilibrium *to* the periodic orbit will itself be of codimension-two while the connection back the other way is generic. Note that, unlike each of the other codimension-two mechanisms we review here which can occur in $\mathbb{R}^3$, an EP2 point requires four phase space dimensions. The asymptotics of how the curve of homoclinic orbits approaches such an EP2 point were studied in [34]. The rate and manner of convergence (i.e., direct or wiggly approach) depends in part on the size of the Floquet multiplier of the periodic orbit and whether the Floquet multipliers are real or complex. A complete unfolding of other codimension-one bifurcation curves nearby is unknown.

(e) Equilibrium-to-periodic heteroclinic tangency (EP1t). In contrast to an EP2 point, here the periodic orbit has a two-dimensional unstable manifold and so the heteroclinic connection

from the equilibrium *to* the periodic orbit is of codimension one, whereas the connection from the periodic orbit *back to* the equilibrium remains generic. A codimension-two point is reached when the generic connection forms a tangency. This case was partially studied in [34], with more details to appear in [9]. In fact such a point does not represent an end-point of a curve of homoclinic orbits: there is an infinite number of homoclinic curves, each of which undergoes a turning point in the parameter plane close to the codimension-two point. Each successive curve corresponds to an orbit with an additional loop near the periodic orbit. Also arising from the codimension-two point are curves of homoclinic tangencies to the periodic orbit that have a complex topology.

(f) A blue-sky catastrophe of homoclinic orbits. This occurs when the homoclinic bifurcation curve ends at a curve of fold bifurcations of periodic orbits. One natural way for such a codimension-two point to arise would be if the saddle-node periodic orbit appears in the stable manifold of the equilibrium to the left of the red Hopf curve in the case where the Hopf bifurcation is subcritical (the small arrows in Fig. 3 indicate the direction of bifurcation). The resulting barrier prevents the existence of a homoclinic orbit, and the homoclinic branch must terminate via the orbit wrapping itself infinitely many times around the emerging structurally unstable periodic orbit. This case is currently being studied [10]. There may be other similar termination mechanisms involving homoclinic wrapping around nonhyperbolic periodic orbits, for example, orbits undergoing a period-doubling bifurcation, but we are not aware of any theoretical analyses.

It is pertinent to point out that homoclinic curves that appear to terminate 'in mid air' in a parameter plane, may in fact not imply the existence of a codimension-two bifurcation point at all. For example, we shall see in several of the examples below cases where the homoclinic bifurcation curve turns around sharply and doubles back on itself as it approaches (but does not quite reach) the Hopf bifurcation. The homoclinic orbit typically gains an extra loop as it does so, so that globally a single-pulse orbit becomes a double-pulse orbit. The sharpness of the turn in the parameter space means that the bifurcation curve appears to terminate, but there is in fact no terminating bifurcation. However, as we shall see, such sharp turns occur naturally as a consequence of some of the other mechanisms listed above, notably the EP1t case.

3   Numerical continuation results

Throughout we use the continuation routines HomCont [11, 12] that are embedded in the software AUTO [15] in order to trace curves of homoclinic orbits in two parameters. AUTO is a numerical bifurcation analysis package, which uses pseudo-arclength continuation in combination with the solution of two-point boundary value problems with Gauss-Legendre collocation. We use the other capabilities of AUTO to trace curves of local bifurcations of equilibria and periodic orbits and to identify codimension-two bifurcation points. The periodic and homoclinic orbits under consideration in this paper are discretized with a total of `NTST`×`NCOL` points, where `NTST` is the number of mesh intervals and `NCOL` the number of so-called Gauss collocation points per mesh interval.

The general method that was used to produce the bifurcation diagrams was as follows: an equilibrium point was determined either analytically or numerically for certain parameter values. This equilibrium was then continued in one parameter, until a Hopf bifurcation was detected. AUTO can both continue this Hopf bifurcation in two parameters and continue a periodic orbit from the Hopf bifurcation in one parameter. The period of the periodic orbit grows to infinity as the homoclinic

orbit is approached. Then the HomCont algorithm can phase-shift such a periodic orbit so that the beginning and end-points are close to the equilibrium and then continue the homoclinic orbit in two parameters using projection boundary conditions.

Note that cases (a) and (e) in Fig. 3 involve interaction of the primary homoclinic curve with homoclinic tangencies to periodic orbits. There are currently no implemented general boundary-value methods for continuation of homoclinic tangencies to periodic orbits in arbitrary dimensions, although see for example [45]. Instead, we can use the result that homoclinic tangencies are accompanied by a sequence of parameter values at which fold bifurcations occur [21, 20]. Therefore, by following folds of high-period periodic orbits that approach a homoclinic tangency we can compute approximations to such global bifurcation curves.

The systems studied in this paper are all highly stiff (with time scales differing by up to 13 orders of magnitude in some cases). This stiffness complicates the computations. For instance, the computation of Floquet multipliers of periodic solutions in AUTO is not very reliable once the system has very small or very large multipliers; see [31]. Of particular significance for the systems in this paper is the observation that detection of homoclinic bifurcations can be difficult in stiff systems. For instance, there may exist periodic orbits with extremely high period that can be misdetected as implying the existence of homoclinic orbits. In such circumstances it is sometimes necessary to increase the number of mesh intervals (`NTST`) to values up to 600 to retain convergence, while a number of about 30 is usually sufficient for non-stiff systems. Similarly, it was sometimes found to be necessary to increase the truncated time interval T over which we compute approximations to homoclinic orbits up to 10^6 to avoid, but still not completely eliminate, false positive results.

3.1   Model 1: FitzHugh-Nagumo

We begin by considering the bifurcation set of the travelling wave FitzHugh-Nagumo system (2) with the parameter values (3), as discussed in the Introduction. Note that equations (2) have a symmetry. Specifically, in the case $\gamma = 1$, $\alpha = 0.1$, the equations are equivariant under the transformation

$$v \to \frac{11}{15} - v, \quad w \to \frac{11}{15} - w, \quad d \to -d, \quad p \to \frac{11}{15}\left[1 - \frac{38}{225}\right] - p, \tag{4}$$

which means that the bifurcation set in the (p, s) plane is symmetric under reflection through the line $p = 0.3047$. Thus there are actually two C-shaped curves of homoclinic bifurcations, one to the left of the Hopf U as shown, and a mirror image to the right of the U (not shown). We discuss only the leftmost C here; results are analogous for the other C.

Detailed numerics reveal that the homoclinic locus that appears to be a single C-curve in Fig. 1 is in reality a pair of curves which join together in two fold-like structures in the parameter plane, forming a closed curve; when the homoclinic branch is followed numerically in the parameters p and s, the branch turns around at one end of the C, then appears to retrace its path to the other end of the C where it turns around again and returns to its starting point. On the scale of Fig. 1, the C appears to be a single curve, and even when zooming in the separation between the curves is hard to see because the distance between curves approaches the numerical accuracy of AUTO/HomCont. However, as shown in Fig. 4, the two curves can be distinguished by plotting the numerically computed L_2-norm along the homoclinic locus. We call the thin closed loop of homoclinic orbits in Fig. 1 a *homoclinic banana*. Thus we see that the homoclinic locus in the FitzHugh-Nagumo system does not terminate at each end in a codimension-two point, as would seem the case from a first

glance at the bifurcation set. This is an example of the *apparent* termination mechanism discussed at the end of Section 2.2. We note that the ends of the C curve have different shapes when the L_2 norm is plotted against p, with the upper end being blunt and involving a number of turning points, while the lower end has, within numerical accuracy, just one sharp turn. Preliminary calculations suggest the existence of *canards*, that is rapid growth from small scale to large scale oscillations in a thin wedge of parameter space, near the upper end of the C curve and this may explain the difference in structure at the two ends.
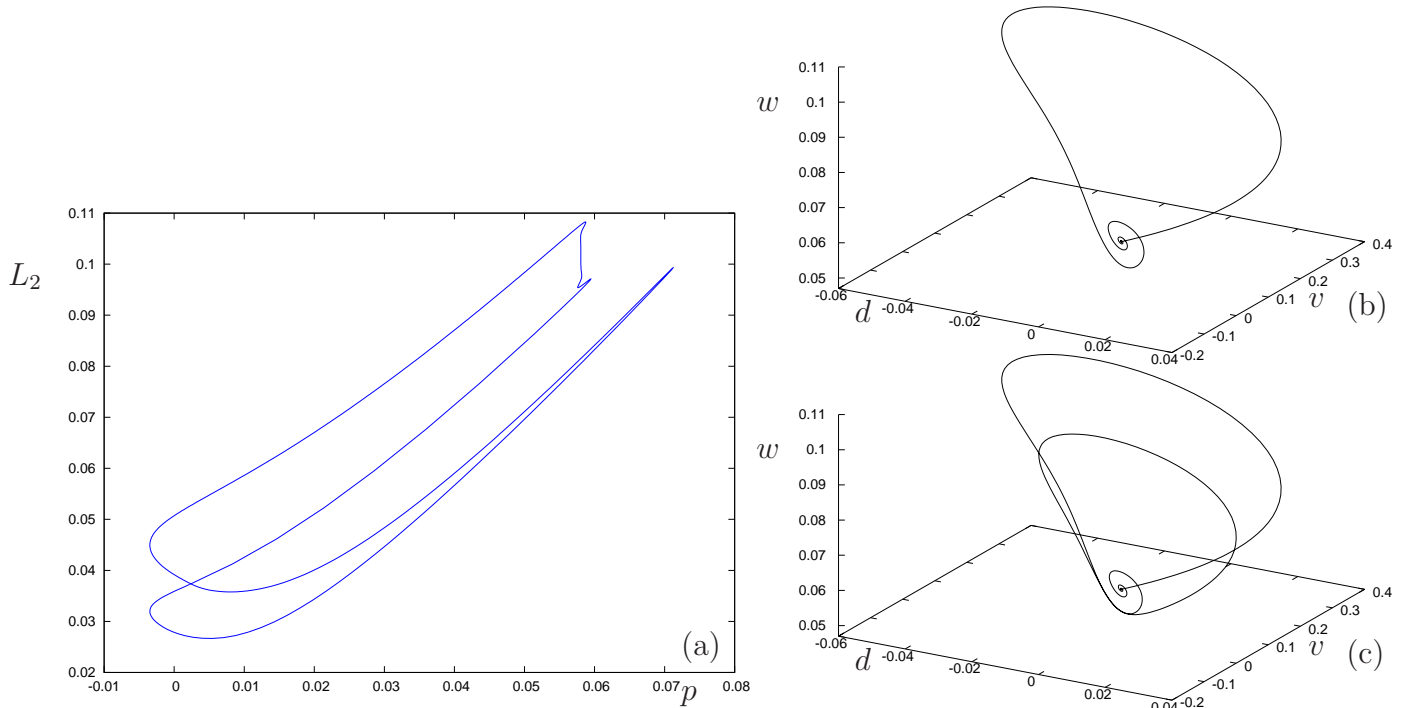

Figure 4: Another projection of the 'homoclinic banana' for the FitzHugh-Nagumo system (2) with the parameters (3) (cf. the C curve in Fig. 1). Panels (b) and (c) show two different homoclinic orbits at $p \approx 0.06$, $s \approx 0.894386$ near the lower end of the banana. Note the gross difference in phase space between these two orbits. We (loosely) refer to the orbit in (b) as a single-pulse orbit and the orbit in (c) as a double-pulse orbit.

Near both ends of the C curve, the Hopf bifurcation is sub-critical, and the periodic orbit created in the Hopf bifurcation appears on the left side of the U. Numerical continuation of this periodic orbit for fixed $s = 1$ produces the dotted wiggly curve shown in Fig. 5. The form of this curve indicates that the periodic orbit approaches a set of homoclinic tangencies to a limit cycle (see e.g. [20]). In particular there are four accumulation points for the saddle-node bifurcations of periodic orbits on the dotted curve in Fig. 5. According to theory, these accumulate on four separate parameter values at which there are tangencies between the stable and unstable manifolds of a hyperbolic limit cycle. We note here that the rate of converge in p of each set of folds to a fixed value is extremely rapid. As each set of four folds is traversed the orbits undergoing this wiggling acquire an extra loop near the limit cycle (see the two sub-panels to the figure which depict orbits with 1 and 5 oscillations per period near the limit cycle, respectively). The limit cycle in question (shown as a dashed curve in Fig. 5) can itself be continued into a Shil'nikov homoclinic orbit. At different parameter values we

might thus expect to see an interaction between homoclinic orbits to an equilibrium and homoclinic tangencies to a periodic orbit.
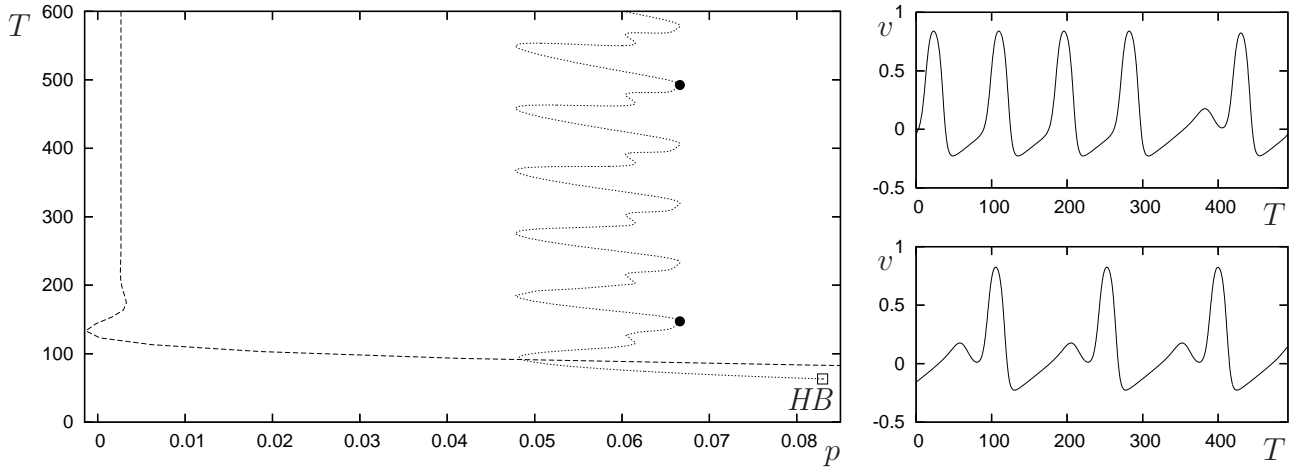

Figure 5: Bifurcation diagram and time series for the FitzHugh-Nagumo model with $s = 1$. Left: bifurcation diagram showing the period T as a function of p. The dashed curve continues beyond the right arm of the Hopf U, eventually terminating in a second homoclinic bifurcation at $p \approx 0.61$. The dotted curve arises from a Hopf bifurcation on the left arm of the Hopf U (bifurcation point marked HB). Right: time series for the periodic orbits with period $T = 492.476$ and $T = 147.184$, indicated by the large dots in the bifurcation diagram.

Figure 5 suggests there is a lot more structure to the bifurcation set for the FitzHugh-Nagumo equations than is shown in Fig. 1. Figure 6 shows some of the additional bifurcations that occur between the C and the U. Note in particular the degenerate Hopf bifurcation marked with a square and the curve of saddle-node bifurcations of a periodic orbit that emanates from this point. Also, some of the saddle-node bifurcations of periodic orbits seen in Fig. 5 have been continued in two parameters and their loci are shown in Fig. 6. We have distinguished between two types of saddle-node bifurcations in the zoom Fig. 6(b). Of particular interest are the purple curves which correspond to the fold bifurcations in Fig. 5 that approach the homoclinic tangencies. Thus the purple curves are approximations to loci of homoclinic tangencies to periodic orbits. The sharp turning point in the blue homoclinic curve occurs very close to the parameter value at which the homoclinic orbit and homoclinic tangency interact. This is an example then of an EP1t equilibrium-to-periodic heteroclinic tangency, which is case (e) of Fig. 3.

It is also instructive to look for Belyakov transitions. It is straightforward to check numerically that, for the parameter values used above, the saddle-quantity of the homoclinic orbits on the C-curve is always positive and the stable leading eigenvalues are always complex. Thus homoclinic bifurcations of the equilibrium in this system always display Shil'nikov-type behaviour and no Belyakov transitions occur. However, for different values of the parameter ε the behaviour changes. As is depicted in Fig. 7, for smaller values of ε there exist two Belyakov transitions on the C-shaped homoclinic bifurcation curve. In between these two Belyakov points, the eigenvalues of the equilibrium are real and there exists just a single homoclinic bifurcation curve. On the right hand side of each Belyakov point the C-curve is in fact a pair of homoclinic bifurcation curves just as for the homoclinic banana above; a single-pulse homoclinic orbit deforms into a double-pulse homoclinic orbit, with the double-pulse orbit then terminating at the Belyakov point. Thus the homoclinic banana is now split. Similar behaviour was found in [33] and [30]. Using HomCont we were able to find the critical value of ε where the behaviour changes and the two Belyakov points appear. This
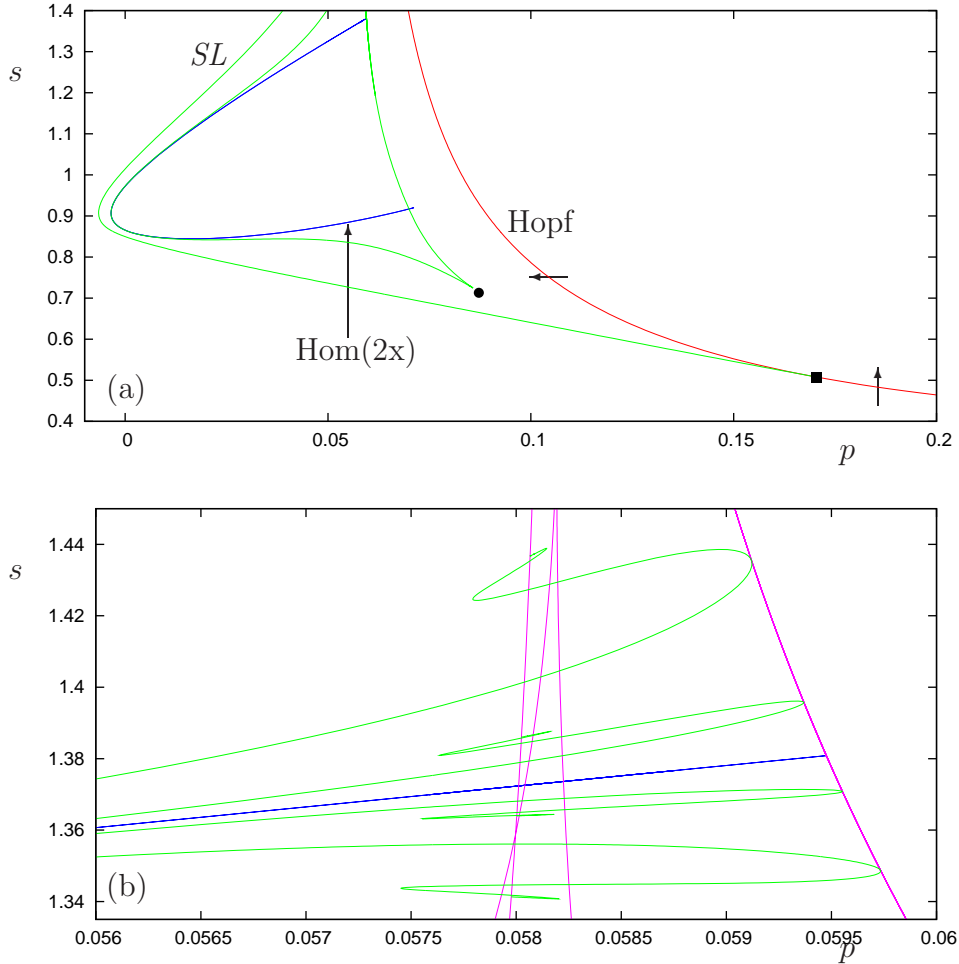
Figure 6: A more detailed bifurcation set for the FitzHugh-Nagumo system. (a) The curve labelled Hom (2x) is the 'homoclinic banana' described in the text. The right-most curve is part of the U-shaped Hopf curve, with the square marking a degenerate Hopf bifurcation and the large dot marking a cusp bifurcation. All other curves denote saddle-node bifurcations of limit cycles. The arrows indicate the direction in which periodic orbits appear on the various sections of the Hopf bifurcation curve. (b) A zoom near the top end of the homoclinic curve. The red curve delineates the homoclinic banana. The green curves show saddle-node bifurcations of limit cycles associated with the unfolding of the codimension-one Shil'nikov bifurcation. The purple curves also show saddle-node bifurcations of periodic orbits, but these are associated with the folds on branches of periodic orbits that approach a homoclinic tangency of a periodic orbit (two such saddle-node bifurcations were marked with large dots in Fig. 5).

codimension-three point, denoting the transition between the banana and the *banana-split* case, occurs at $\varepsilon = 0.006018385$ for $p = -0.05314325$ and $s = 0.07101599$.

In summary, we have gained some insight into the termination of the homoclinic bifurcation curve in the travelling-wave FitzHugh-Nagumo equations, namely: the C curve does not terminate at each end but instead folds back on itself, with the single-pulse homoclinic orbit deforming into a double-pulse orbit in the process. One way of explaining the sharp turning points of the homoclinic curve is through the numerical evidence we have presented for the existence of equilibrium-to-periodic heteroclinic tangencies (EP1t points). The intricate dynamics near the EP1t point, in particular the interaction between fold curves and homoclinic tangencies will be discussed further in [9]. Note though that things are made even more subtle by the slow-fast nature of the FitzHugh-Nagumo model and the consequent occurrence of canard-like behaviour.
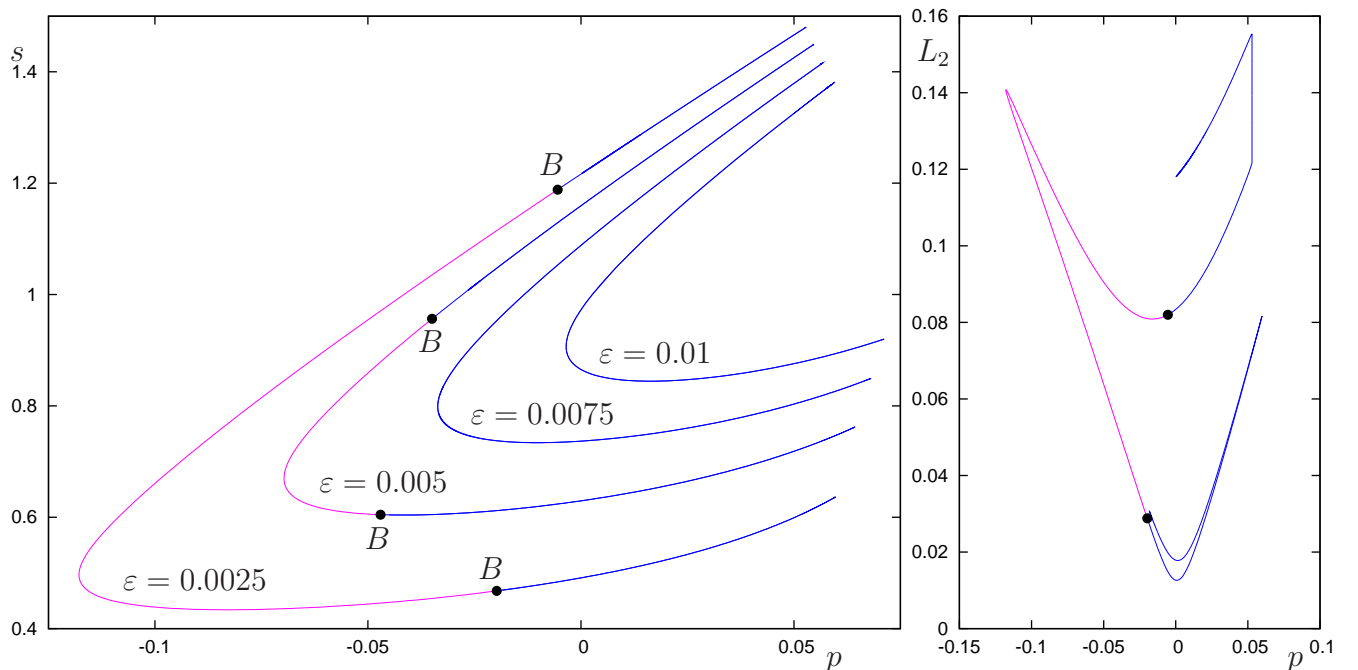

Figure 7: Homoclinic bifurcation curves in parameter space for different values of ε in the FitzHigh-Nagumo system. There exist Belyakov transitions (marked B) on the curves corresponding to $\varepsilon = 0.0025$ and $\varepsilon = 0.005$ (the banana-split case), whereas on the other curves no Belyakov transitions occur (the banana case). On the left side of the Belyakov points the eigenvalues of the equilibrium are real rather than complex. Right: L_2-norm for the homoclinic orbits occurring along the banana-split curve in the case $\varepsilon = 0.0025$. This panel demonstrates that each point on the C-shaped curve between the Belyakov points corresponds to a single homoclinic bifurcation curve, while to the right of each Belyakov point there are two curves of homoclinic bifurcations.

3.2 Model 2: Sneyd, LeBeau and Yule three variable model

In [41] a model of intracellular calcium wave propagation in pancreatic acinar cells was constructed and studied. Two versions of this model were considered; after passage to travelling wave coordinates one model has three phase space variables and the other four. In this section we look at the former (SLY-3), and in the next section at the latter (SLY-4). For more details on the construction of these models, the interested reader is referred to the original paper.
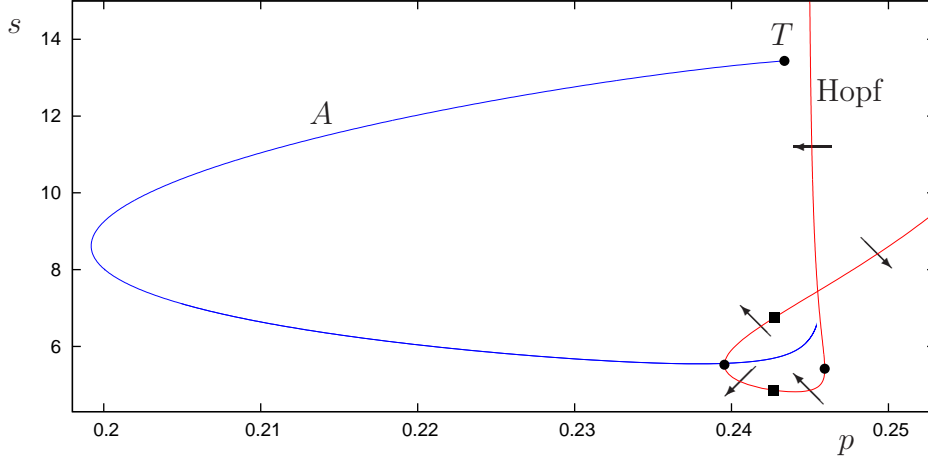
14

Figure 8: Partial bifurcation set for the SLY-3 model, equations (5), showing the CU nature of the bifurcation curves. The two arms of the Hopf U cross one another, forming a loop, with the arrows denoting the directions in which periodic orbits appear in the Hopf bifurcation. The dots on the Hopf locus denote saddle-node Hopf bifurcations and the squares mark degenerate Hopf bifurcations. The C-shaped homoclinic bifurcation curve (labelled A following the notation of [41]) terminates at the top at a T-point (labelled T), and turns around sharply at the lower end in the same way as the lower end of the C curve in the FitzHugh-Nagumo equations.

The SLY-3 model equations are given by:

$$\begin{aligned}
\dot{c} &= d \\
D_c\dot{d} &= sd - k_f\left(\frac{ph\varphi_1}{\varphi_1 p + \varphi_{-1}}\right)^4 + \frac{V_p c^2}{K_p^2 + c^2} - J_{\text{leak}} \\
s\dot{h} &= \varphi_3(1-h) - \left(\frac{\varphi_1\varphi_2 p}{\varphi_1 p + \varphi_{-1}}\right)h.
\end{aligned} \tag{5}$$

Here c denotes the calcium concentration, s is the wave speed introduced when moving to travelling wave coordinates, and p represents the concentration of inositol trisphosphate (IP$_3$), a second messenger that can be experimentally controlled, at least to a certain extent. All other quantities in the equations are either constant or functions of c; see Appendix A for details. We are interested in the bifurcation set in the (p, s) parameter plane. Much of the bifurcation set for this model was described already in [41], with some further details in [37, 8]. This example is presented here as an illustration of two of the five mechanisms (i.e., T-point and Fold-Hopf) by which homoclinic loci terminate near Hopf bifurcations in CU systems. Several new relevant bifurcation results are also included.

There are four main homoclinic branches in this system. One of these, named branch A following the notation of [41], is shown in Fig. 8 together with the locus of Hopf bifurcations. We regard this system as a CU system even though the two arms of the Hopf U cross each other forming a loop as shown in Fig. 8. The Hopf bifurcation is degenerate at $s \approx 4.858$ and at $s \approx 6.7502$, and the direction in which the bifurcating periodic orbit appears on each section of the Hopf bifurcation curve is indicated in the figure.

At the upper end of the C-shaped curve, branch A terminates at a T-point, as described in [41]. An interesting result about dynamics near the T-point was proved in [35], where it was shown that stable pulses in the underlying partial differential equations arise from the gluing together of two
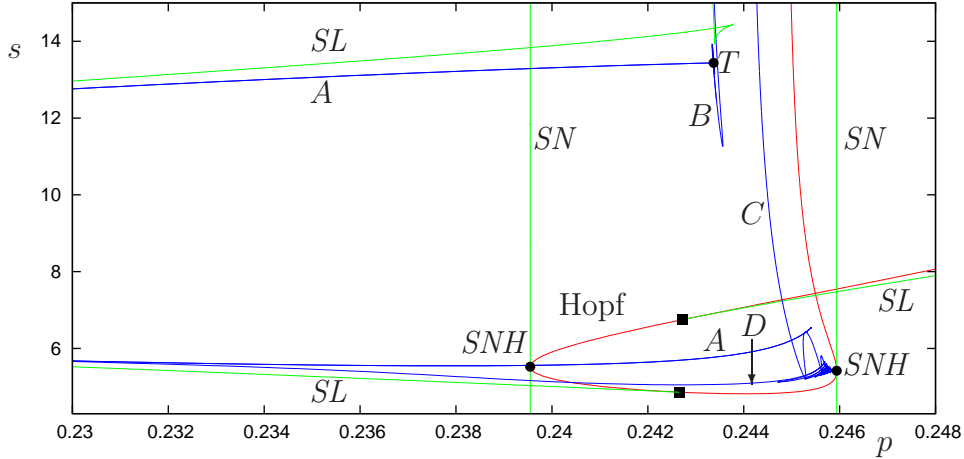
Figure 9: A more detailed bifurcation set for the SLY-3 model. This figure is an enlargement of part of Fig. 8. Depicted are the homoclinic bifurcations A, B, C, and D, the two saddle-node bifurcations of equilibria SN, the two saddle-node Hopf bifurcations SNH, the T point, and the two saddle-node bifurcations of limit cycles SL which terminate at the degenerate Hopf bifurcations marked with squares.

unstable fronts. At the lower end of the C-shaped curve, the branch of homoclinic bifurcations makes a tight turn, and the homoclinic orbit deforms continuously from a single-pulse orbit to a double pulse orbit, in a similar way to that seen near the lower end of the C curve in the FitzHugh-Nagumo model. The branch of double-pulse orbits then doubles back all the way to the T-point, terminating at or very near the T-point. Thus, once again we find the C-shaped curve is a homoclinic banana, although in this case one end of the banana is attached to the T-point. We note that the banana-nature of branch A is a new result. In [41] it was conjectured that branch A terminates near the Hopf bifurcation when the amplitude of the homoclinic orbit goes to zero. On the other hand, [37] showed that branch A had a sharp turning point at the lower end of the C curve but was able to trace the doubled-back curve only as far as the large bend in the C at $(p, s) \approx (0.2, 8.5)$. This is an example of the way in which the extreme stiffness of the CU models considered in this paper can result in misleading numerical results, even when great care is taken in the numerical simulations.

Three further curves of homoclinic bifurcations (branches B to D) are shown along with branch A in Fig. 9. Branch B starts at the T-point; in Fig. 9 it leaves the diagram in the direction of increasing s and will not concern us further. Branch C starts at a saddle-node Hopf point and does not terminate; it also leaves the bifurcation set in the direction of large s. Branch D starts at the same saddle-node Hopf point as branch C (it wiggles around branch C; see [8]) and then follows branch A, finally terminating at the T-point.

There are other curves of homoclinic bifurcations besides the four branches, A to D, identified above. For instance, if we follow one of the double pulse orbits that lie close to the branch A, we find that it too originates from the T-point. In the other direction these branches follow branch A towards the SNH point, but turn around sharply just before this point and return to the T-point again.

16

3.3 Model 3: Sneyd, Le Beau, and Yule four variable model

The SLY-4 model, studied in [41], is given by the following system of equations:

$$
\begin{aligned}
\dot{c} &= d \\
D_c \dot{d} &= sd - k_f y^4 + \frac{V_p c^2}{K_p^2 + c^2} - J_{\text{leak}} \\
s\dot{x} &= p\varphi_1 x - \varphi_{-1} y - \varphi_2 y \\
s\dot{y} &= -(p\varphi_1 x - \varphi_{-1} y) + \varphi_3 (1 - x - y).
\end{aligned}
\tag{6}
$$

The variable h in SLY-3 is related to x and y in SLY-4 by $h = x + y$, with all other variables, parameters and expressions in SLY-4 the same as for SLY-3, as detailed in Appendix A.

A partial bifurcation set for this system is shown in Fig. 10. The bifurcations seen are similar to those in the FitzHugh-Nagumo system. In particular, the C-shaped curve is a homoclinic banana as for the FitzHugh-Nagumo equations. There is also a saddle-node bifurcation of periodic orbits emanating from a degenerate Hopf bifurcation, and homoclinic bifurcations of periodic orbits. Fig. 10(b) shows bifurcations of one branch of periodic orbits associated with SLY-4; compare with Fig. 5.

This example does not exhibit any new mechanisms for termination of the homoclinic branches, but does show that two closely-related models (SLY-3 and SLY-4) can have completely different termination mechanisms for the branch of homoclinic bifurcations. Why this should be so is not clear. Nevertheless, it is apparent that minor changes in model structure, ones that have little to no significant effect on model behaviour over the vast majority of parameter space, can cause significant qualitative changes in certain sensitive areas of parameter space. Although it is unlikely that such changes in the bifurcation structure would be reflected in experimental results, or lead to testable predictions, it is still necessary to understand the complete range of possibilities in order to develop a proper mathematical understanding of the CU structure.
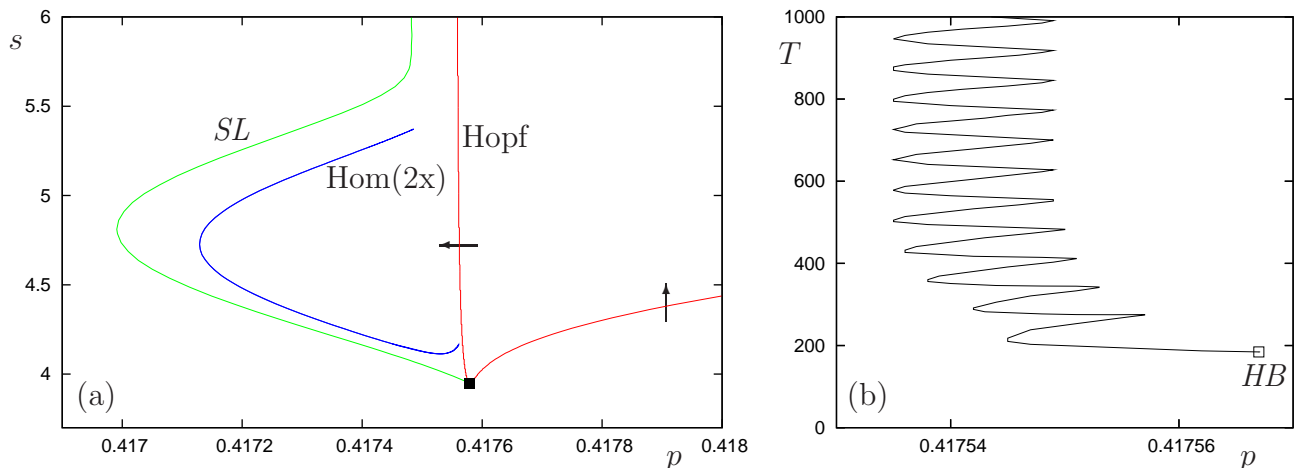

Figure 10: (a) A partial bifurcation set for the SLY-4 model, equations (6). The curve labelled Hom (2x) represents a homoclinic banana. The square on the Hopf curve marks a degenerate Hopf bifurcation. All other curves are saddle-node bifurcations of limit cycles. The arrows through the Hopf locus indicate the direction in which periodic orbits appear on the various sections of the Hopf bifurcation curve. (b) Bifurcation diagram for the SLY-4 model, for $s = 4.17$, showing the branch of periodic orbits that emanates from the Hopf bifurcation in panel (a).

3.4 Model 4: A nine-dimensional calcium model

The equations we consider in this section come from a model for calcium wave propagation in pancreatic acinar cells developed in [40] and [43] and further studied in [38]. After passage to a moving frame of reference, we obtain the travelling wave equations for the model:

$$
\begin{aligned}
\dot{c} &= d \\
D_c \dot{d} &= sd - J \\
s\dot{c}_e &= (J_{\text{serca}} - (k_f P_{\text{IPR}} + \nu_1 P_{\text{ryr}} + J_{\text{er}})(c_e - c))\gamma \\
s\dot{R} &= \varphi_{-2}O - \varphi_2 pR + (k_{-1} + l_{-2})I_1 - \varphi_1 R \\
s\dot{O} &= \varphi_2 pR - (\varphi_{-2} + \varphi_4 + \varphi_3)O + \varphi_{-4}A + k_{-3}S \\
s\dot{A} &= \varphi_4 O - (\varphi_{-4} + \varphi_5)A + (k_{-1} + l_{-2})I_2 \\
s\dot{I}_1 &= \varphi_1 R - (k_{-1} + l_{-2})I_1 \\
s\dot{I}_2 &= \varphi_5 A - (k_{-1} + l_{-2})I_2 \\
s\dot{w} &= k_{\text{cm}}(w_\infty - w)/w_\infty,
\end{aligned}
\tag{7}
$$

where $J \equiv (k_f P_{\text{IPR}} + \nu_1 P_{\text{ryr}} + J_{\text{er}})(c_e - c) - J_{\text{serca}} - J_{\text{mito}} + \delta(J_{\text{in}} - J_{\text{pm}})$. Here c_e denotes the concentration of calcium ions in the endoplasmic reticulum, R denotes the fraction of receptors in various states, and $\delta = 0.1$ controls the magnitude of trans-membrane fluxes relative to the trans-ER fluxes without resting $[\text{Ca}^{2+}]$. The other parameters and constants are given in Appendix A.
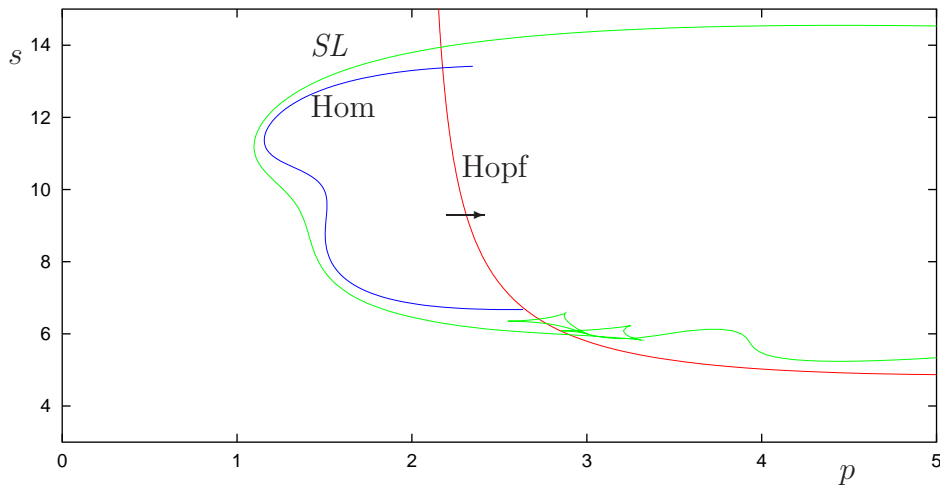

Figure 11: Partial bifurcation set for the nine-dimensional calcium model, equations (7). The C curve of homoclinic bifurcations appears to cross the Hopf bifurcation curve at one end, but this is believed to be a numerical artifact as explained in the text. At the other end, the C curve turns around sharply at the first in a sequence of sharp turns which are not visible in this figure. There are no degenerate points on the Hopf locus; the saddle-node bifurcation of limit cycles (curve marked SL) does not terminate in this figure.

Figure 11 shows a partial bifurcation set for this system of equations. At the lower end of the C-shaped homoclinic locus, the homoclinic branch has a sharp turning point, with the branch doubling back on itself. Unlike the case in the earlier example systems in which the turning point caused a homoclinic banana, here we have something topologically very different; see Fig. 12. Here the homoclinic branch follows an (infinite) sequence of turning points that accumulate on two extreme values of (p, c). The turning points actually separate into six sets of points with four intermediate sets of folds between the extrema (which are the only sets that are easily visible in Fig. 12(a)).

As we move through one complete cycle of six folds, the homoclinic orbit gains an extra large loop. As this process continues the orbit transforms from a primary Shil'nikov homoclinic orbit (Fig. 12(b)) to something that increasingly resembles a heteroclinic cycle between the equilibrium point and a periodic orbit (Fig. 12(c)). Note that Fig. 12(a) shows the L_2-norm computed by AUTO as a function of p; in a plot of c vs. p all the separate folds of the branch fall on top of one another to within numerical accuracy. The AUTO L_2-norm is defined as $(1/T) \int_0^T \|u\|^2 dt$, where T is a fixed large time over which the homoclinic orbit is computed. Since the equilibrium has a higher L_2 value than the periodic orbit, the L_2-norm for fixed T *decreases* in Fig. 12(a) as more turns are added around the periodic orbit. Behaviour of this type is explained in Ref. [9]. Each of the accumulation points of the folds of the homoclinic locus corresponds to an EP1t-point, and the global connectedness of the locus is due to the topology of the intersection between the stable manifold of the equilibrium and the unstable manifold of the periodic orbit.

In Fig. 11 the top end of the homoclinic locus seems to pass straight through the Hopf bifurcation curve and terminate at $p \approx 2.3$! However, we believe this to be a numerical artifact and that the homoclinic curve actually terminates at a Shil'nikov/Hopf bifurcation when the homoclinic locus reaches the Hopf locus. This numerical anomaly is due to the slow-fast nature of the system; a detailed discussion is deferred to section 3.6.
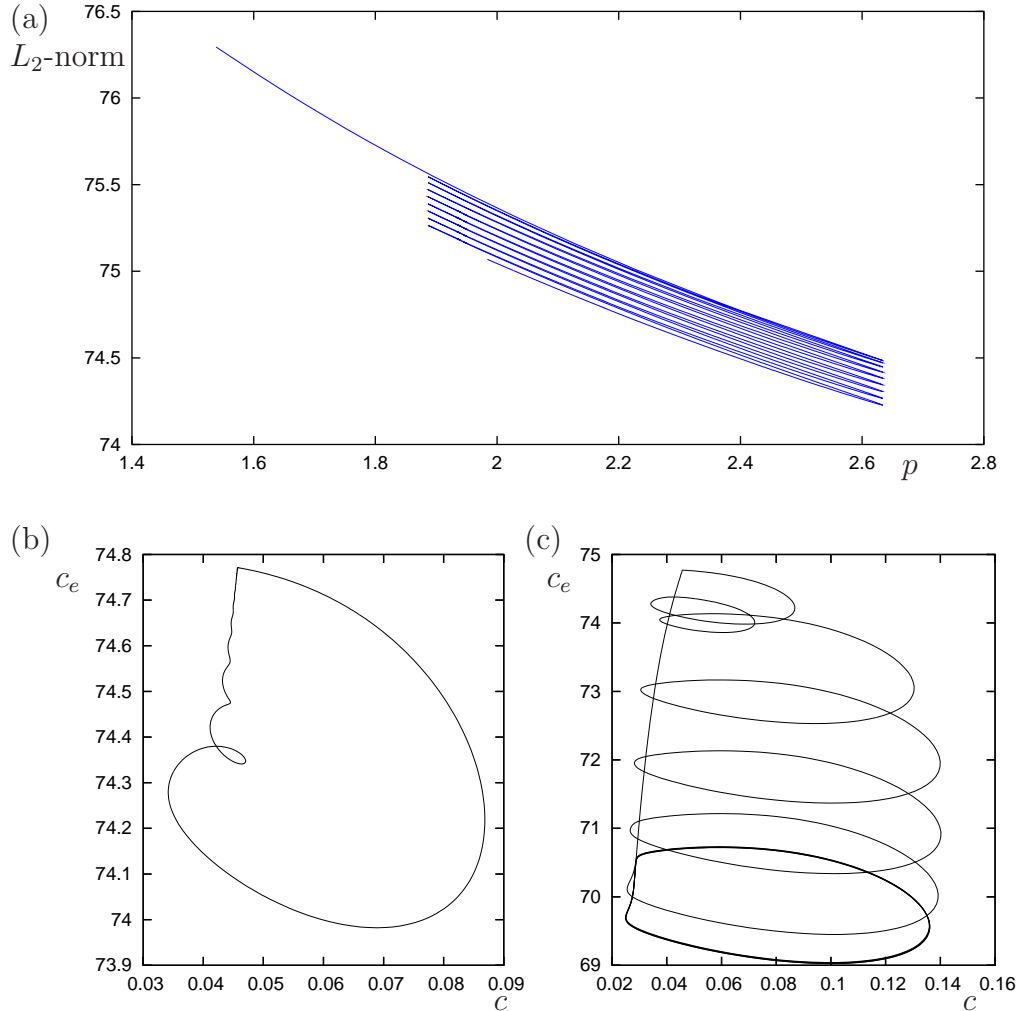
Figure 12: (a) Detail along the lower part of the homoclinic branch in Fig. 11, showing the L_2-norm of the homoclinic orbit as a function of p. The turning points on the homoclinic branch initially approximately alternate between two locations, with p values given approximately by 2.63466, 1.88681, 2.63383, 1.88681, 2.63383 and 1.88681, and then follow a repeated sequence of six values of p: 2.63383, 1.93415, 1.93954, 1.88681, 1.95014, 1.94495. Not all turning points can be distinguished in the figure. Below: Homoclinic orbits near the lower end of the homoclinic branch. (b) The homoclinic orbit before going through any turning points, at $(p, s) = (2.4, 6.68342)$; (c) the homoclinic orbit at approximately the same place in parameter space, at $(p, s) = (2.4, 6.68342)$ after going through 17 outer turning points.

3.5 Model 5: A four-dimensional simplification

Assuming fast equilibration between all the receptor states except R and A, we can reduce equations (7) to a model with only a single gating variable, but one whose steady-state behaviour is equivalent to (7):

$$\dot{c} = d$$
$$D_c\dot{d} = sd - ((J_{\text{IPR}} + J_{\text{er}})(c_e - c) - J_{\text{serca}} + \delta(J_{\text{in}} - J_{\text{pm}}))$$
$$\dot{c}_t = \delta(J_{\text{in}} - J_{\text{pm}})$$
$$s\dot{R} = -\varphi_5 A + (k_{-1} + l_{-2})(1 - R).$$

$$(8)$$

Here the variable c_t is related to the variables in (7) via the equation $c_t = sc_e/\gamma - D_c d + sc$. All other variables, parameters and constants in these equations have the same meaning as in equations (7).
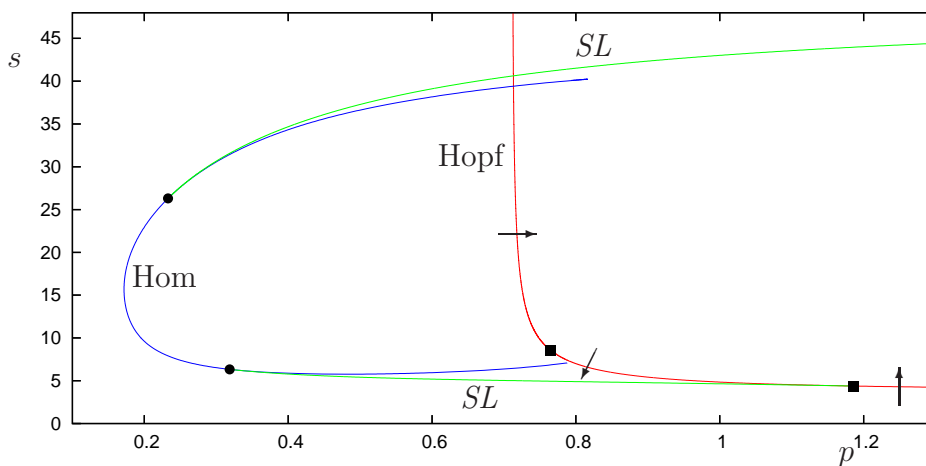

Figure 13: Partial bifurcation set for the four-dimensional calcium model, equations (8). The homoclinic bifurcation curve appears to cross the Hopf locus at the top end, but this is believed to be a numerical artifact, as discussed in the text. At the lower end the homoclinic locus goes through a sequence of sharp turning points, eventually converging at a codimension-two point at $p = 0.7682935$. The two curves of saddle-node bifurcations of periodic orbits (marked SL) terminate on the homoclinic bifurcation curve at the large dots where the leading eigenvalues of the corresponding equilibrium resonate: the saddle quantity of the saddle vanishes at these points. The lower SL bifurcation terminates at its right end at a degenerate Hopf bifurcation, indicated by a square. A second degenerate Hopf bifurcation lies to the left, just above the lower end of the C curve; the SL curve emanating from this degenerate Hopf bifurcation is not shown. The arrows indicate the direction of the Hopf bifurcation as in Fig. 6.

Figure 13 shows a partial bifurcation set for equations (8). The top end of the homoclinic branch has similar behaviour to that seen in the nine-dimensional model, with the numerical approximation to the homoclinic locus crossing the Hopf bifurcation curve. Again, we believe this to be a numerical artifact but return to a fuller discussion of the phenomenon in section 3.6.

Behaviour near the lower end of the homoclinic curve is different in this system than in the nine-dimensional model. As before, the branch initially turns around sharply, and there follows a series of further sharp turns, but the turning points converge to a single point rather than to two (see Fig. 14). Again as in the nine-dimensional model, the homoclinic orbit looks increasingly like a heteroclinic
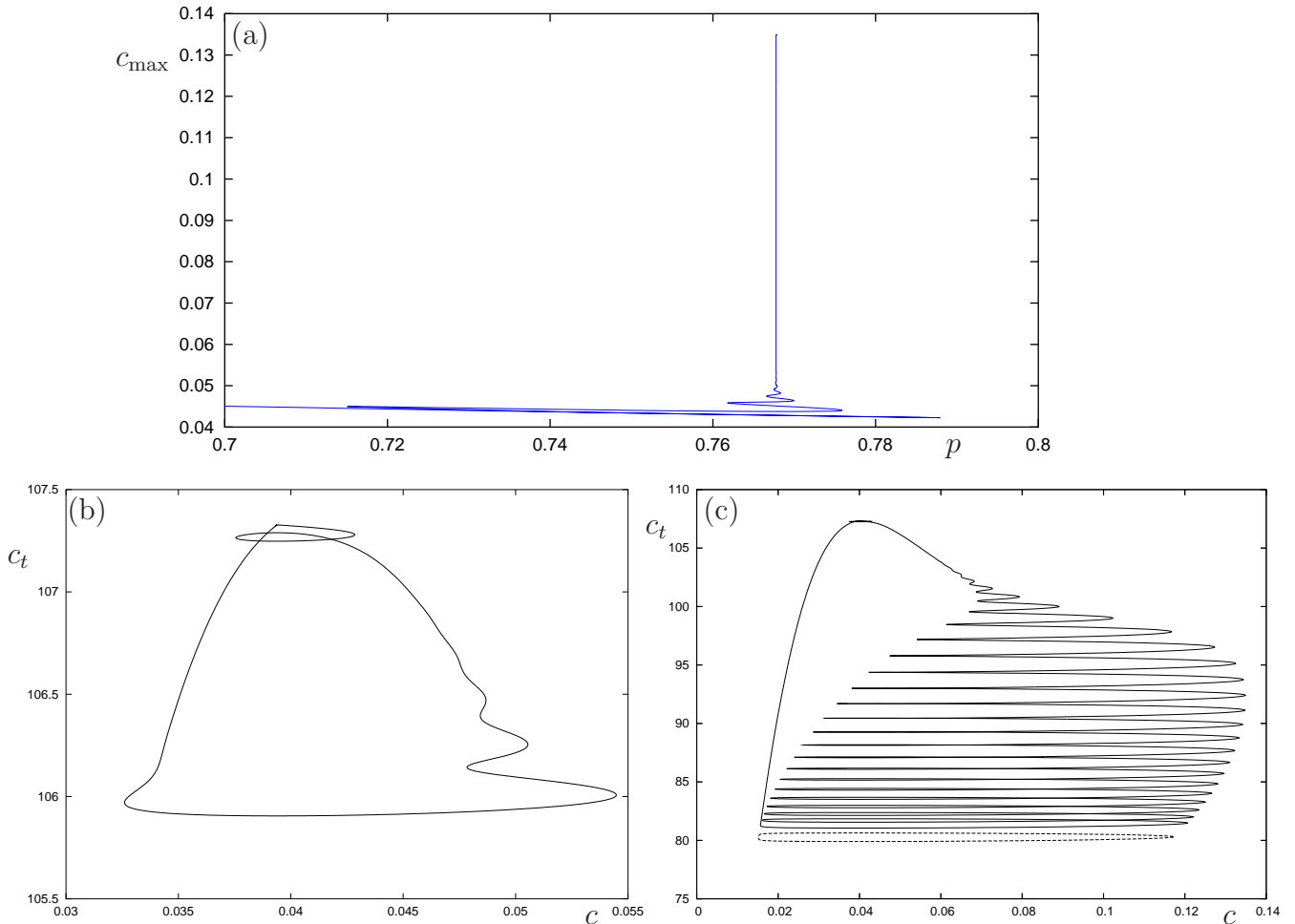
Figure 14: (a) The lower part of the homoclinic bifurcation curve in the four-dimensional calcium model, equations (8), showing the maximum value of c on the homoclinic orbit, c_{max}, as a function of p. After many turns c_{max} stabilises at 0.134922. (b) The homoclinic orbit at $p = 0.7682935$ after 15 turns of the homoclinic bifurcation curve. (c) The homoclinic orbit at $p = 0.7682935$ after many turns of the homoclinic bifurcation curve. Also plotted (dashed curve) is a periodic orbit that bifurcates from the right arm of the U-shaped Hopf locus. This orbit was obtained by continuing in p for s fixed from the Hopf bifurcation point at $(p, s) = (22.04131, 6.878683)$.

cycle between the equilibrium and a periodic orbit as we move along the folded homoclinic branch (see Figs 14(b) and 14(c)). We conjecture that the turning points in the homoclinic bifurcation curve are organized here by a codimension-two heteroclinic bifurcation involving the equilibrium and the periodic orbit. The oscillatory approach to this codimension-two point is reminiscent of an EP2 point (case (d) in Fig. 3). However, at the time of writing it is not clear whether this is the case, or whether we have another example of the phenomenon in Fig. 12, explained by the presence of several EP1t points, with remarkably thin wiggles at large periods.

The chief difference between the EP1t and EP2 heteroclinic cycles is the dimension of the stable manifold of the periodic orbit. Indeed, the rate of convergence of the turning points near either an EP2 or an EP1t point was found in [34] to depend on the Floquet multipliers of the periodic orbit. However, due to the stiffness of the equations we have been unable to calculate these multipliers accurately enough to compare numerics with the theory. (AUTO calculations give the Floquet multipliers of the periodic orbit as $1, 0.28, 8 \times 10^{-7}, -1 \times 10^{6}$, but these multipliers cannot be trusted since the signs are clearly wrong. However, from these calculations it appears that the

periodic orbit, as followed from the Hopf bifurcation, does not undergo any bifurcations and has consistently two multipliers strictly inside the unit circle, suggesting an EP1t point).

A significant difference between this case and the nine-dimensional model is that in these equations the Hopf bifurcation is subcritical near the lower end of the homoclinic branch, producing a periodic orbit to the left of the Hopf locus, although it is not clear whether this has any bearing on the question of how the homoclinic branch terminates.

3.6   Model 6: A five-dimensional variant

The model studied in this section is another simplification of the nine-dimensional model described in section 3.4; instead of using a six-state model of the IPR as in equations (7), all but three of the states are assumed to be in instantaneous equilibrium and a fast time scale reduction is applied to simplify the model. The reduced, five-dimensional model is given by the following set of equations:

$$
\begin{aligned}
\dot{c} &= d \\
D_c \dot{d} &= sd - [(k_{\mathrm{f}} P_{\mathrm{IPR}} - J_{\mathrm{er}})(c_e - c) - J_{\mathrm{serca}} + \delta(J_{\mathrm{in}} - J_{\mathrm{pm}})] \\
s\dot{c_e} &= -\gamma \left[(k_{\mathrm{f}} P_{\mathrm{IPR}} - J_{\mathrm{er}})(c_e - c) - J_{\mathrm{serca}} \right] \\
s\dot{O} &= \phi_2 pR - \theta_1 O + (k_{-1} + l_{-2})I_2 - \theta_2 O \\
s\dot{R} &= \theta_1 O - \phi_2 pR.
\end{aligned}
\tag{9}
$$

All parameters and constants in these equations are given in Appendix A. This system of equations was studied in [22, 23], where a partial bifurcation diagram for this system (Fig. 15) was obtained. In this figure, the homoclinic bifurcation curve appears to overshoot the Hopf bifurcation curve at both ends by a significant amount, in a similar way to that seen near the upper ends of the C-shaped curves in Figs. 11 and 13. (Note that the Hopf bifurcation is supercritical for all values of p and s in this figure.) Since there is only one equilibrium solution to equations (9), there must be a homoclinic-Hopf bifurcation of the equilibrium solution at the point where the homoclinic and Hopf bifurcation curves coincide. Just to the left of the Hopf bifurcation locus, we generically expect that the homoclinic orbit will enter the equilibrium solution along a direction tangent to the center manifold. The dynamics associated with such a homoclinic-Hopf bifurcation in a three-dimensional system is described in [26], while [13] discusses the case in three or higher dimensions. In both papers it is shown that the homoclinic bifurcation curve terminates at the Hopf locus. To understand why the numerically computed homoclinic bifurcation curve shown in Fig. 15 overshoots the Shil'nikov-Hopf point it is necessary to look a little closer at the algorithms used to obtain the numerical approximation to the homoclinic locus. We do so below, but note that much of this discussion was also contained in [23].

Homoclinic bifurcation curves like those shown in Fig. 15 can be obtained using any algorithm that sets up well-posed boundary conditions after truncation to a (large) finite time interval $t \in (0, T)$. For example, HomCont poses projection boundary conditions based on eigenvectors of the adjoint linearised problem about the equilibrium point. The dimensions of the stable and unstable subspaces are fixed at the beginning of the computation. In a case such as ours, where these dimensions change mid-computation (as the Hopf locus is crossed) HomCont will continue to compute an orbit that satisfies the specified boundary conditions even though the boundary conditions are no longer appropriate. Thus, if using HomCont to compute the approximate homoclinic locus for equations (9), we must ignore any part of the computed curve located inside the U-shaped Hopf
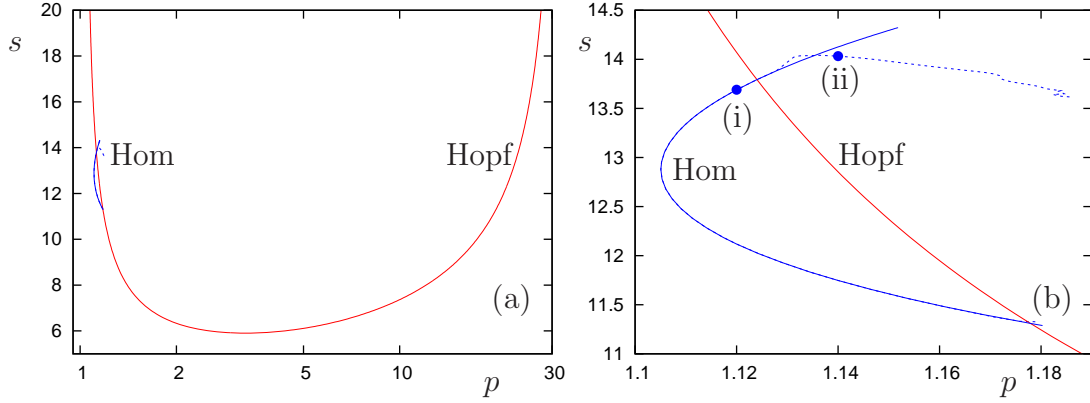
Figure 15: (a) Partial bifurcation set for the five-dimensional model, equations (9). (b) An enlargement of part of (a). Homoclinic and Hopf bifurcations are labelled. The points labelled (i) and (ii) in (b) correspond to the parameters used for the phase portraits in Fig. 16. In (b) two different algorithms are used to compute the homoclinic curve: projection boundary conditions (solid line) and fixed period-5000 periodic orbit (dashed line). To the left of the Hopf line these two curves are overlaid to the accuracy depicted.
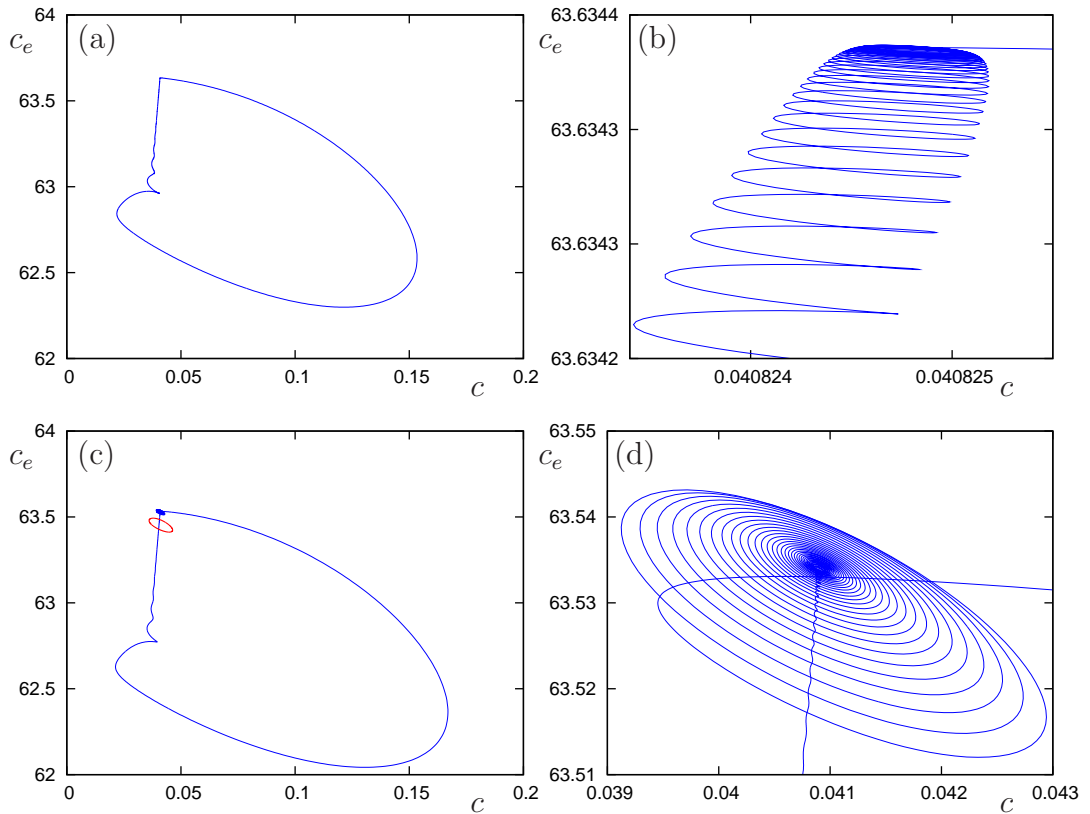
Figure 16: Phase portraits at the points labelled (i) and (ii) in Fig. 15, computed with AUTO by following an orbit of fixed period (period 5000) with AUTO constant `NTST=1000`. (a) At point (i); (b) enlargement of (a) near the equilibrium. (c) At point (ii). The red curve is the periodic orbit created in the Hopf bifurcation; (d) enlargement of (c) near the equilibrium.

locus; the computed curve in this region apparently approximates a heteroclinic connection from the equilibrium to the Hopf periodic orbit rather than a homoclinic bifurcation of the equilibrium.

More details on the HomCont algorithm can be found in [12].

An alternative approximation to the homoclinic locus may be obtained using periodic boundary conditions, and following a periodic orbit of fixed high period (say period 5000 or higher). This method is known to be less accurate than using projection boundary conditions, but nevertheless converges as $T \to \infty$ to the correct result. The approximate homoclinic locus for equations (9) obtained with this method is indicated by the dashed curve in Fig. 15(b); like the case with projection boundary conditions, this curve also crosses the Hopf locus at each end. However, examination of the phase portraits at various points on the curve suggests that the locus of homoclinic bifurcations of the equilibrium terminates at the Hopf locus, just as expected from a Shil'nikov-Hopf bifurcation. Panels (a) and (b) in Fig. 16 show the period 5000 orbit approximating the homoclinic orbit at a point to the left of the Hopf bifurcation (point (i) in Fig. 15(b)), while panels (c) and (d) show the orbit at point (ii) in Fig. 15(b). It is clear from the figure that after the Hopf bifurcation, instead of simply spiralling in towards the equilibrium point, the computed orbit spirals *out* towards the period orbit (shown as a red curve in Fig. 15). Thus we are actually computing an approximation to a heteroclinic connection from the equilibrium to the periodic orbit created in the Hopf bifurcation, rather than a true homoclinic orbit to the equilibrium. In this case, it appears that high period orbits persist beyond the Hopf bifurcation even though the homoclinic bifurcation terminates at the Hopf locus.

From detailed examination of the phase portraits for this model it is evident that the true homoclinic locus terminates at the Hopf bifurcation at both upper and lower ends. These are just regular Shil'nikov-Hopf bifurcation points (case (a) of Fig. 3). We conjecture that exactly the same process occurs in the 4D and 9D models (7) and (8), at the upper end of the C-branch, where the homoclinic locus appears to cross the Hopf bifurcation curve. These equations are even more stiff than the present 5D model and even detailed examination of the phase portraits fails to reveal that the computation of the homoclinic branch has become spurious upon crossing the Hopf U. The difficulty in these cases appears to be the presence of a slow manifold in the associated phase space. Most models of calcium dynamics, including all the CU-systems studied here, have slow manifolds that are important in determining the dynamics. (A comprehensive review of models of calcium waves is given in [16], while a detailed discussion of slow manifolds in this context, as well as in the context of more generic excitable system theory, can be found in [28].)

In the three models (equations (7), (8) and (9)) the slow manifold is one-dimensional and passes through the single equilibrium, with the motion on the slow manifold being toward the equilibrium. A homoclinic orbit in these systems typically leaves the equilibrium along the unstable manifold and makes a global excursion, before being drawn into a tiny tube around the slow manifold. It then follows the slow manifold toward the equilibrium until it gets close enough that the dynamics on the center manifold takes over. If the equilibrium solution is attracting within the center manifold, the orbit will then approach the equilibrium solution in a direction tangent to the center manifold, thereby closing the homoclinic connection. If, however, the equilibrium has undergone a supercritical Hopf bifurcation and is unstable, it can take a remarkably long time before the trajectory along the slow manifold reaches sufficiently close to the equilibrium to experience this instability. As a result, if one uses a high-period periodic orbit approximation to the homoclinic orbit, with insufficiently high period, the computed orbit may not reach the center manifold at all before leaving the equilibrium. In such a case, the dominant feature of the center manifold dynamics, namely outward spiralling from the equilibrium, will not be observed.

Based on the above discussion, we conjecture that the mechanism for the termination of the upper end of the C-shaped curves in equations (7) and (8) and both ends of the C-curve in equations (9) is simply the Shil'nikov-Hopf bifurcation.

4 Discussion

We have studied a hierarchy of detailed models of excitable systems, focusing in particular on those that model calcium dynamics. The main aim of the work has been to understand the connection between two different dynamical regimes for which travelling-wave type behaviour is observed in these systems, and in particular to look at the interaction between small-amplitude waves born in a Hopf bifurcation in the travelling wave equations, and solitary pulses represented by homoclinic orbits in the travelling wave equations. We have found that this interaction can occur in a variety of different ways, despite broad similarities in behaviour in the models we have analysed. It seems that there are many different ways in which Shil'nikov chooses to meet Hopf!

Specifically, we have sought codimension-two mechanisms for the termination of homoclinic bifurcation curves as they approach a Hopf bifurcation. In our examples we have identified cases of T-points, saddle-node/Hopf local bifurcations, and equilibrium-to-periodic heteroclinic bifurcations. We also found Shil'nikov-Hopf bifurcations in a number of cases; these bifurcations were unusually numerically delicate because of the degree of stiffness in the model equations, with the consequence that in each case the homoclinic bifurcation curve appeared at first analysis to pass through the Hopf locus instead of terminating there, as theory would predict. We argued that this behaviour is a numerical artifact, and gave a plausibility argument as to why even very careful numerics near Shil'nikov-Hopf bifurcations can be misleading whenever slow manifolds are present. Proper multiple time-scale analysis of this behaviour is left for future work.

The stiffness of the models we studied most likely plays an important role in other terminating mechanisms besides the Shil'nikov-Hopf bifurcation. For instance, we found that rapid, canard-like growth of oscillations occurs near the blunt end of the homoclinic banana in the FitzHugh-Nagumo equations. An investigation of the role of canards in calcium models is the subject of ongoing work.

A number of our models contained an apparent codimension-two termination mechanism, where a codimension-one homoclinic bifurcation curve appeared to terminate 'in mid air'. In each case, in turned out that the bifurcation curve was not actually terminating but rather going through a sharp turn and doubling back on itself, but with the doubled-back curve being indistinguishable from the original curve on the scale of the bifurcation diagram; typically the homoclinic orbit gained an extra loop in the process so that a single-pulse orbit became a double-pulse orbit. Such sharp turns require no special explanation in terms of bifurcation theory, but are important within our taxonomy of termination mechanisms since they arise naturally as a consequence of some of the other mechanisms, as described earlier.

We do not, at present, fully understand the significance of the sub- or supercriticality of the Hopf bifurcation in these systems. A better understanding may follow from forthcoming theoretical work on homoclinic orbits to degenerate Hopf points [10].

We have not considered here the PDE stability of the travelling wave structures we have identified. Generally in these types of models it is the upper branch of the C-curve of homoclinic bifurcations that is of physiological interest as this corresponds (in the PDE) to stable pulses while the other branches correspond to unstable pulses. The significance of the details of our codimension-two termination mechanisms for the PDE dynamics is unclear. For instance, given the strong contractions due to the slow-fast nature of the dynamics, the precise details of the spurious passage through the Shil'nikov-Hopf bifurcations may not be important; something that is exponentially close to a homoclinic orbit on the 'wrong side' of the Hopf bifurcation may in fact imply the existence of an almost steady travelling pulse for exponentially long times. It would be of interest, therefore, to see if the Hopf bifurcation in these cases might not be 'felt' at all in PDE computations of stable

travelling pulses over finite timescales, in the same way that its presence was almost undetectable when tracing paths of homoclinic bifurcations to the travelling wave ODEs.

The detailed numerics we have presented are for two distinct types of excitable system, the FitzHugh-Nagumo equations which might be regarded as the canonical excitable system, and a class of models of the dynamics of intracellular calcium. We expect that many of the features we have found will also be relevant to other classes of excitable systems, for example, models of heart tissue and neural oscillators.

A   Parameters and formulae for model definitions

The following constants and quantities were used in numerical simulations of models 2 and 3 (SLY-3 and SLY-4):

k_f	J_{leak}	k_1	k_2	k_3	k_{-1}	V_p	K_p	r_2	r_4	r_6	r_{-2}	R_1	R_3	R_5	D_c
28	0.2	0	0.53	1	0.88	1.2	0.18	100	20	0	0	6	50	1.6	25

$$\varphi_{-1} = (k_{-1} + r_{-2})R_3/(c + R_3)$$
$$\varphi_1 = (k_1 R_1 + r_2 c)/(R_1 + c)$$
$$\varphi_2 = (k_2 R_3 + r_4 c)/(R_3 + c)$$
$$\varphi_3 = (k_3 R_5 + r_6 c)/(R_5 + c).$$

The following constants and quantities were used in numerical simulations of models 4, 5, and 6 (nine-, four and five-dimensional models):

J_{inbase}	k_f	J_{er}	γ	V_{serca}	K_{serca}	V_{pm}	K_{pm}	δ	D_c	ν_1	V_{mito}
0.2	0.32	0.002	5.405	120.0	0.18	28.0	0.425	0.1	20	0.04	0

In the four-dimensional model 5 we used the values $D_c = 25$ and $k_f = 0.4$ instead of the above values.

k_{ap}	k_{am}	k_{bp}	k_{bm}	k_{cp}	k_{cm}
1500	28.8	1500	385.9	1.75	0.1

k_1	k_{-1}	k_2	k_{-2}	k_3	k_{-3}	k_4	k_{-4}	l_2	l_6	L_1	L_5	l_4	L_3
0.64	0.04	37.4	1.4	0.11	29.8	4	0.54	1.7	4707	0.12	54.7	1.7	0.025

$$K_a = (k_{\mathrm{am}}/k_{\mathrm{ap}})^{\frac{1}{4}}$$

$$K_b = (k_{\mathrm{bm}}/k_{\mathrm{bp}})^{\frac{1}{3}}$$

$$K_c = k_{\mathrm{cm}}/k_{\mathrm{cp}}$$

$$w_\infty = \frac{1 + (K_a/c)^4 + (c/K_b)^3}{1 + 1/K_c + (K_a/c)^4 + (c/K_b)^3}$$

$$J_{\mathrm{mito}} = V_{\mathrm{mito}}\frac{c^3}{1 + c^2}$$

$$P_{\mathrm{ryr}} = w\frac{1 + (c/K_b)^3}{1 + (K_a/c)^4 + (c/K_b)^3}$$

$$P_{\mathrm{IPR}}(O, A) = (O/10 + 9A/10)^4 \ (\text{model } 4)$$

$$P_{\mathrm{IPR}}(O) = O^4\theta_3 \ (\text{model } 6)$$

$$S = 1 - R - O - A - I_1 - I_2$$

$$J_{\mathrm{in}} = J_{\mathrm{inbase}} + 0.05p$$

$$l_{-2} = l_2 k_{-1}/(k_1 L_1) \ (\text{models } 4 \text{ and } 5)$$

$$l_{-2} = 0.8 \ (\text{model } 6)$$

$$l_{-6} = k_{-4}l_6/(k_4 L_5) \ (\text{models } 4 \text{ and } 5)$$

$$l_{-6} = 11.4 \ (\text{model } 6)$$

$$l_{-4} = k_{-2}l_4/(k_2 L_3) \ (\text{models } 4 \text{ and } 5)$$

$$l_{-4} = 2.5 \ (\text{model } 6)$$

$$\varphi_1(c) = \frac{(k_1 L_1 + l_2)c}{L_1 + c(1 + L_1/L_3)}$$

$$\varphi_2(c) = \frac{k_2 L_3 + l_4 c}{L_3 + c(1 + L_3/L_1)}$$

$$\varphi_{-2}(c) = \frac{k_{-2} + l_{-4}c}{1 + c/L_5}$$

$$\varphi_3(c) = \frac{k_3 L_5}{L_5 + c}$$

$$\varphi_4(c) = \frac{(k_4 L_5 + l_6)c}{L_5 + c}$$

$$\varphi_{-4}(c) = \frac{L_1(k_{-4} + l_{-6})}{L_1 + c}$$

$$\varphi_5(c) = \frac{(k_1 L_1 + l_2)c}{L_1 + c}$$

$$\Phi_2 = \varphi_{-2}/\varphi_2$$

$$\Phi_4 = \varphi_{-4}/\varphi_4$$

$$A = pR/(p + \Phi_2\Phi_4 + p\Phi_4)$$

$$J_{\mathrm{IPR}} = k_f A^4$$

$$J_{\mathrm{pm}}(c) = \frac{V_{\mathrm{pm}}c^2}{K_{\mathrm{pm}}^2 + c^2}$$

$$J_{\mathrm{serca}}(c, c_e) = \frac{V_{\mathrm{serca}}c}{c_e(K_{\mathrm{serca}} + c)}$$

$$\theta_1(c) = \frac{0.5 + 0.5c^2}{0.36 + 20c^2}$$

$$\theta_2(c) = \frac{8.1c^2}{0.2 + 5c^2}$$

$$\theta_3(c) = \frac{0.00074 + 8.6c^2}{0.74 + 13c^2}$$

$$I_2 = 1 - R - O \ (\text{model } 6 \text{ only}).$$

References

[1] L.A. Belyakov. Bifurcation of systems with homoclinic curve of a saddle-focus with saddle quantity zero. *Mat. Zam.* 36 (1984) 838–843.

[2] L.A. Belyakov. The bifurcation set in a system with a homoclinic saddle curve. *Mat. Zam.* 28 (1980) 910–916.

[3] L.A. Belyakov. A case of the generation of a periodic motion with homoclinic curves. *Mat. Zam.* 15 (1974) 336–341.

[4] M.J. Berridge, M.D. Bootman and H.L. Roderick. Calcium signalling: dynamics, homeostasis and remodelling. *Nat. Rev. Mol. Cell. Biol.* 4 (2003) 517–529.

[5] H.W. Broer and G. Vegter. Subordinate Shil'nikov bifurcations near some singularities of vector fields having low codimension. *Ergod. Theory Dynam. Sys.* 4 (1984) 509–525.

[6] V.V. Bykov. Bifurcations of dynamical systems close to systems with a separatrix contour containing a saddle-focus. In *Methods of the Qualitative Theory of Differential Equations*, E.A. Leontovich-Andronova (Ed) (1980) 44-72 Gor'kov. Gos. Univ., Gorki.

[7] V.V. Bykov. The bifurcations of separatrix contours and chaos. *Physica D* 62 (1993) 260–299.

[8] A.R. Champneys and V. Kirk, The entwined wiggling of homoclinic curves emerging from saddle-node/Hopf instabilities. *Physica D* 195 (2004) 77–105.

[9] A.R. Champneys, V. Kirk, E. Knobloch, B. Oldeman and J. Rademacher. Equilibrium to periodic orbit heteroclinic tangencies. Preprint 2007.

[10] A.R. Champneys, V. Kirk and E. Knobloch. Blue sky catastrophies of homoclinic orbits. In preparation, 2007.

[11] A.R. Champneys and Yu.A. Kuznetsov. Numerical detection and continuation of codimension-two homoclinic bifurcations. *Int. J. Bifurcation and Chaos* 4 (1994) 785–822.

[12] A.R. Champneys, Yu.A. Kuznetsov and B. Sandstede. A numerical toolbox for homoclinic bifurcation analysis. *Int. J. Bifurcation and Chaos* 6 (1996) 867–887.

[13] B. Deng and K. Sakamoto. Šil'nikov-Hopf bifurcations. *J. Diff. Eqns.* 119 (1995) 1–23.

[14] E.J. Doedel, A.R. Champneys, T.F. Fairgrieve, Y.A. Kuznetsov, B. Sandstede, and X. Wang. AUTO 97: Continuation and bifurcation software for ordinary differential equations. `http://indy.cs.concordia.ca/auto/main.html`

[15] E.J. Doedel, R.C. Paffenroth, A.R. Champneys, T.F. Fairgrieve, Yu.A. Kuznetsov, B.E. Oldeman, B. Sandstede and X. Wang 200. AUTO 2000: Continuation and Bifurcation Software for Ordinary Differential Equations (with HomCont). `http://sourceforge.net/projects/auto2000/`.

[16] M. Falcke. Reading the patterns in living cells - the physics of Ca^{2+} signaling. *Adv. Physics* 53 (2004) 255–440.

[17] C. Fall, E.S. Marsland, J.M. Wagner and J.J. Tyson (Eds). *Computational Cell Biology*, Springer-Verlag, New York, 2002.

[18] R. FitzHugh. Impulses and physiological states in theoretical models of nerve membrane. *Biophys. J.* 1 (1961) 445–446.

[19] P. Gaspard. Local birth of homoclinic chaos. *Physica D* 62 (1993) 94–122.

[20] P. Gaspard and X.-J. Wang. Homoclinic orbits and mixed-mode oscillations in far-from-equilibrium systems. *J. Stat. Phys.* 48 (1987) 151–199.

[21] N.K. Gavrilov and L.P. Shilnikov. On three-dimensional systems close to systems with a structurally unstable homoclinic curve. *Mat. USSR Sb.* 17 (1972) 467–485 & 19 (1973) 139–156.

[22] E. Gin. A bifurcation analysis of calcium buffering. MSc thesis, The University of Auckland, 2005.

[23] E. Gin, V. Kirk and J. Sneyd. A bifurcation analysis of calcium buffering. To appear in *Journal of Theoretical Biology*, 2006.

[24] D.R. Giovannucci, J.I. Bruce, S.V. Straub, J. Arreola, J. Sneyd, T.J. Shuttleworth and D.I. Yule. Cytosolic Ca^{2+} and Ca^{2+}-activated Cl^- current dynamics: insights from two functionally distinct mouse exocrine cells. *J. Physiol.* 540 (2002) 469–484.

[25] P.A. Glendinning and C. Sparrow. T-points: a codimension two heteroclinic bifurcation. *J. Stat. Phys.* 43 (1986) 479–488.

[26] P. Hirschberg and E. Knobloch. Šil'nikov-Hopf bifurcation. *Physica D* 62 (1993) 202–216.

[27] A. L. Hodgkin and A. F.Huxley. A quantitative description of membrane current and its applications to conduction and excitation in nerve. *J. Physiol.* 117 (1952) 500–544.

[28] J. Keener and J. Sneyd. *Mathematical Physiology.* Springer-Verlag, New York, 1998.

[29] Yu.A. Kuznetsov. *Elements of Applied Bifurcation Theory.* Springer-Verlag, New York, 1995.

[30] Yu.A. Kuznetsov, O. De Feo and S. Rinaldi. Belyakov homoclinic bifurcations in a tritrophic food chain model. *SIAM Journal on Applied Mathematics* 62 (2002) 462–487.

[31] K. Lust. Improved numerical Floquet multipliers. *Int. J. Bifurcation and Chaos* 11 (2001) 2389–2410.

[32] J.S. Nagumo, S. Arimoto and S. Yoshizawa. An active pulse transmission line simulating nerve axon. *Proc. IRE* 50 (1962) 2061–2070.

[33] B.E. Oldeman, A.R. Champneys and B. Krauskopf. Homoclinic branch switching: A numerical implementation of Lin's method. *Int. J. Bifurcation and Chaos* 10 (2003) 2977–2999.

[34] J.D.M. Rademacher. Homoclinic orbits near heteroclinic cycles with one equilibrium and one periodic orbit. *J. Diff. Eqns.* 218 (2005) 390–443.

[35] M.M. Romeo and C.K.R.T. Jones. The stability of travelling calcium pulses in a pancreatic acinar cell. Physica D 177 (2003) 242–258.

[36] M. Krupa, B. Sandstede and P. Szmoylan. Fast and slow waves in the FitzHugh-Nagumo equation. *J. Diff. Eqns.* 133 (1997) 49-97.

[37] J. Sim. Saddle-node/Hopf bifurcations in a physiological model. MSc thesis, The University of Auckland, 2002.

[38] D. Simpson, V. Kirk and J. Sneyd. Complex oscillations and waves of calcium in pancreatic acinar cells. *Physica D* 200 (2005) 303–324.

[39] L.P. Shilnikov, A.L. Shilnikov, D.V. Turaev, and L.O. Chua. *Methods of Qualitative Theory in Nonlinear Dynamics, Part II.* World Scientific, Singapore, 2001.

[40] J. Sneyd and J.F. Dufour. A dynamic model of the type-2 inositol trisphosphate receptor. *Proc. Natl. Acad. Sci. USA* 99 (2002) 2398–2403.

[41] J. Sneyd , A. LeBeau and D. Yule. Travelling waves of calcium in pancreatic acinar cells: model construction and bifurcation analysis. *Physica D* 145 (2000) 158–179.

[42] J. Sneyd and K. Tsaneva-Atanasova. Modeling calcium waves. *Lecture Notes in Physics* 623 (2003) 179–199.

[43] J. Sneyd, K. Tsaneva-Atanasova, J.I.E. Bruce, S.V. Straub, D.R. Giovannucci and D.I. Yule. A model of calcium waves in pancreatic and parotid acinar cells. *Biophys. J.* 85 (2003) 1392–1405.

[44] A.V. Tepikin and O.H. Petersen. Mechanisms of cellular calcium oscillations in secretory cells. *Biochim. Biophys. Acta* 1137 (1992) 197–207.

[45] K. Yagasaki. Numerical detection and continuation of homoclinic points and their bifurcations for maps and periodically forced systems. *Int. J. Bifurcation Chaos* 8 (1998) 1617–1627.